An Oligocene ductile strike-slip shear zone: The Uludağ Massif, northwest Turkey—Implications for the westward translation of Anatolia

A.I. Okay[†]
Avrasya Yerbilimleri Enstitüsü ve Jeoloji Mühendisliği Bölümü, Maden Fakültesi, Istanbul Teknik Üniversitesi, Maslak, 34469 Istanbul, Turkey

M. Satır
Institut für Geowissenschaften, Universität Tübingen, Wilhelmstrasse 56, D-72074 Tübingen, Germany

M. Zattin
W. Cavazza
Dipartimento di Scienze della Terra e Geologico-ambientali, Università di Bologna, 40126 Bologna, Italy

G. Topuz
Avrasya Yerbilimleri Enstitüsü, Istanbul Teknik Üniversitesi, Maslak, 34469 Istanbul, Turkey

ABSTRACT

The Uludağ Massif in northwest Turkey represents an exhumed segment of an Oligocene ductile strike-slip shear zone that is over 225 km long and has ~100 km of right-lateral strike-slip displacement. It forms a fault-bounded mountain of amphibolite-facies gneiss and intrusive Oligocene granites. A shear-zone origin for the Uludağ Massif is indicated by: (1) its location at the tip of the active Eskişehir oblique-slip fault, (2) pervasive subhorizontal mineral lineation in the gneisses with a right-lateral sense of slip, (3) foliation with a consistent strike, (4) the presence of a subvertical synkinematic intrusion, and (5) the alignment of the Eskişehir fault, synkinematic metagranite, and the strike of the foliation and mineral lineation. The shear zone nucleated in amphibolite-facies gneisses at peak pressure-temperature (*P-T*) conditions of 7.0 kbar and 670 °C, and it preserves Eocene (49 Ma) and Oligocene (36–30 Ma) Rb/Sr muscovite and biotite cooling ages. The shear zone was active during the latest Eocene and Oligocene (38–27 Ma), as shown by the crystallization and cooling ages from synkinematic granite. A 27 Ma postkinematic granite marks the termination of shear-zone activity. The 20–21 Ma apatite fission-track (AFT) ages indicate rapid exhumation during the early Miocene. A 14 Ma AFT age from an Uludağ gneiss clast deposited in a neighboring Neogene basin shows that the shear zone was on the surface by the late Miocene. Results of this study indicate that during the Oligocene, crustal-scale right-lateral strike-slip faults were transporting crustal fragments from Anatolia into the north-south–extending Aegean; this implies that the westward translation of Turkey, related to the Hellenic slab suction, started earlier than the Miocene Arabia-Eurasia collision.

Keywords: ductile shear zone, strike-slip faulting, Rb/Sr ages, apatite fission tracks, amphibolite-facies metamorphism, Turkey, Aegean Sea.

INTRODUCTION

Active tectonics in the Eastern Mediterranean are dominated by the westward translation of the Anatolian plate into the north-south–extending Aegean region (Fig. 1). Extension in the Aegean region is caused by the southward migration of the Hellenic subduction zone and dates back at least to 30 Ma (late Oligocene; e.g., Jolivet and Faccenna, 2000). In contrast, the North Anatolian fault is regarded to have formed in the late Miocene (ca. 11 Ma) following the collision of the Arabian and Anatolian plates (e.g., Hubert-Ferrari et al., 2002; Şengör et al., 2005). The collision of the Arabian and Anatolian plates is widely considered to be Miocene in age based on the biostratigraphy of the foreland sequences and the transition from marine to continental deposition on the northern margin of the Arabian plate (e.g., Şengör et al., 1985; Dewey et al., 1986; Yılmaz, 1993; Robertson and Grasso, 1995). Global positioning system (GPS) velocities, with respect to the stable Eurasia, show an increase from the Anatolia (~21 mm/yr) toward the Hellenic subduction zone (~33 mm/yr; Reilinger et al., 2006), suggesting that it is not the push from Arabia but rather the pull from slab suction that is driving the present westward translation of the Anatolian plate. What was the tectonic regime in Anatolia during the Oligocene before the Arabia collision? Here, we document the presence of a major Oligocene strike-slip shear zone that has an estimated right-lateral offset of 100 ± 20 km in Anatolia. The Uludağ shear zone, located ~80 km south of the present North Anatolian fault, along with some other strike-slip faults recently shown to have been active in Oligocene times (Aksoy, 1998; Zattin et al., 2005; Uysal et al., 2006), allowed early westward translation of Anatolia. Apart from its regional significance, the shift of localized strain from one major strike-slip fault to another has implications for the rigid versus viscous behavior of the continental lithosphere over geological time scales.

A second aim of the paper is to describe the evolution and exhumation of a major ductile strike-slip shear zone by means of geological mapping combined with stratigraphic, structural, petrologic, and thermochronologic data. Although strike-slip faults are common structures in the continental crust, their roots, i.e., the ductile strike-slip shear zones, are rarely

[†]E-mail: okay@itu.edu.tr.

GSA Bulletin; July/August 2008; v. 120; no. 7/8; p. 893–911; doi: 10.1130/B26229.1; 14 figures; 5 tables.

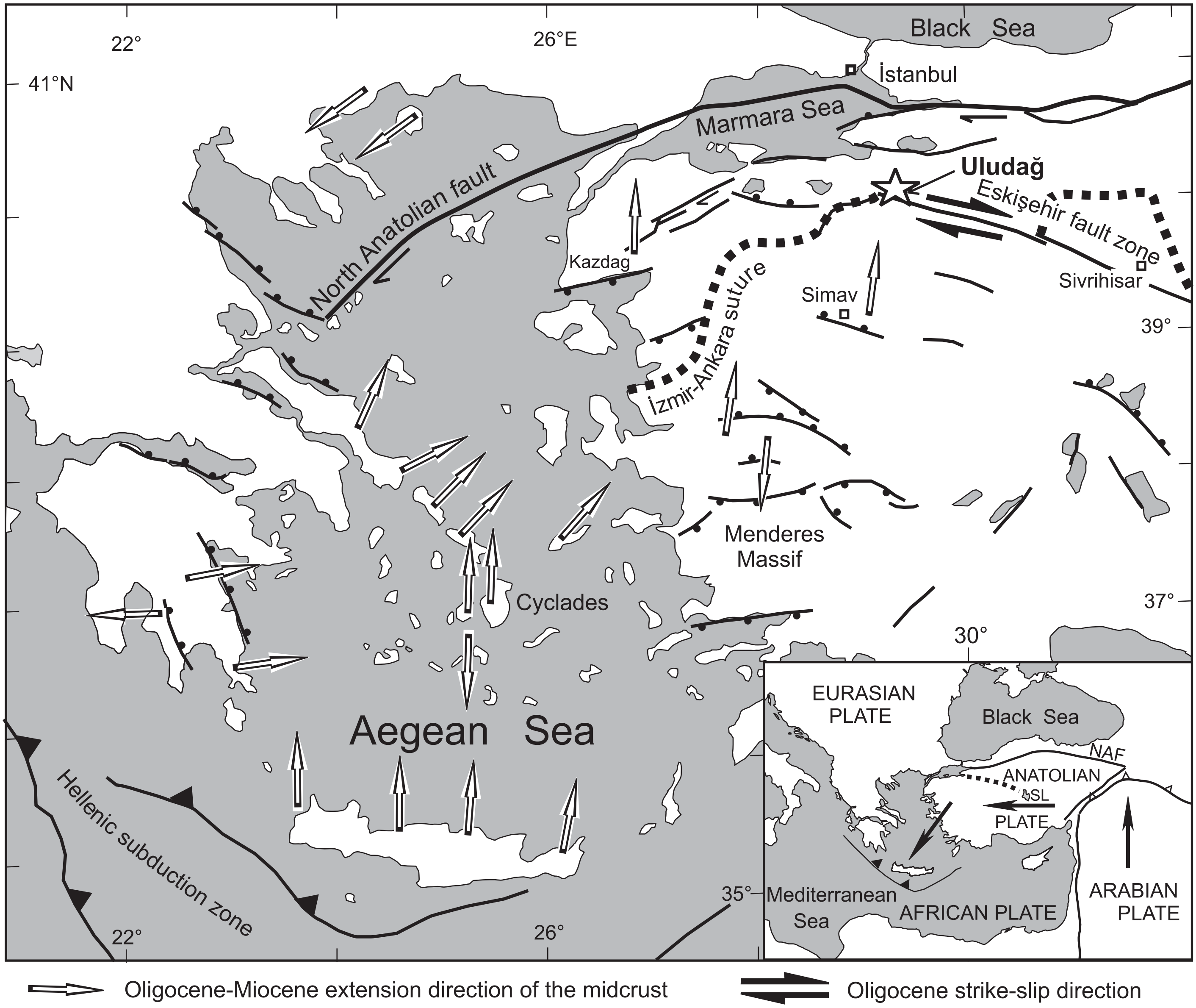

Figure 1. Tectonic map of the Aegean region. The location of the Uludağ Massif is shown by a star. The Oligocene-Miocene ductile extension directions are from Jolivet et al. (2004). The inset shows the active tectonic framework in the Eastern Mediterranean; arrows indicate the present plate movements with respect to Eurasia. The dotted line in the inset denotes the Eskişehir fault zone; NAF—North Anatolian fault; SL—Salt Lake.

exposed. The predominantly horizontal movement typical for strike-slip kinematics generally precludes exhumation of the shear zones, unlike the case of major normal faults, which are frequently associated with ductilely deformed extensional metamorphic core complexes. Some known examples of ductile strike-slip shear zones are the Alpine fault in New Zealand (e.g., Walcott, 1998), the Red River shear zone in southeast Asia (e.g., Tapponnier et al., 1990; Leloup et al., 1993; Anczkiewicz et al., 2007), and the Armorican shear zones in France (e.g., Gapais and Le Corre, 1980; Jégouzo, 1980).

TECTONIC SETTING

The Anatolian microplate is moving westward with respect to the Eurasian plate at a velocity of ~21 mm/yr (e.g., Reilinger et al., 2006). In central Anatolia, over 90% of this movement is concentrated on the North Anatolian fault, which forms a well-defined narrow plate boundary. However, in the Aegean region, the rigid westward translation of the Anatolian microplate gives way to distributed north-south extension along east-west–trending normal faults (Fig. 1). The Uludağ (Ulu Mountain) region is located at the transition zone between the internally rigid Anatolian block and the north-south–extending Aegean (e.g., Şengör et al., 1985; Bozkurt, 2001). The region is characterized by Neogene basins surrounded by mountainous uplands (Fig. 2). The Uludağ is the largest and highest of these uplifted areas; it forms an ESE-trending mountain range, the ancient Mount Olympus of Mysia, which rises to 2543 m above the alluvial Bursa Plain (located at less than 100 m elevation) (Fig. 3).

Uludağ consists of a single east-southeast–trending (~117°) mountain range surrounded

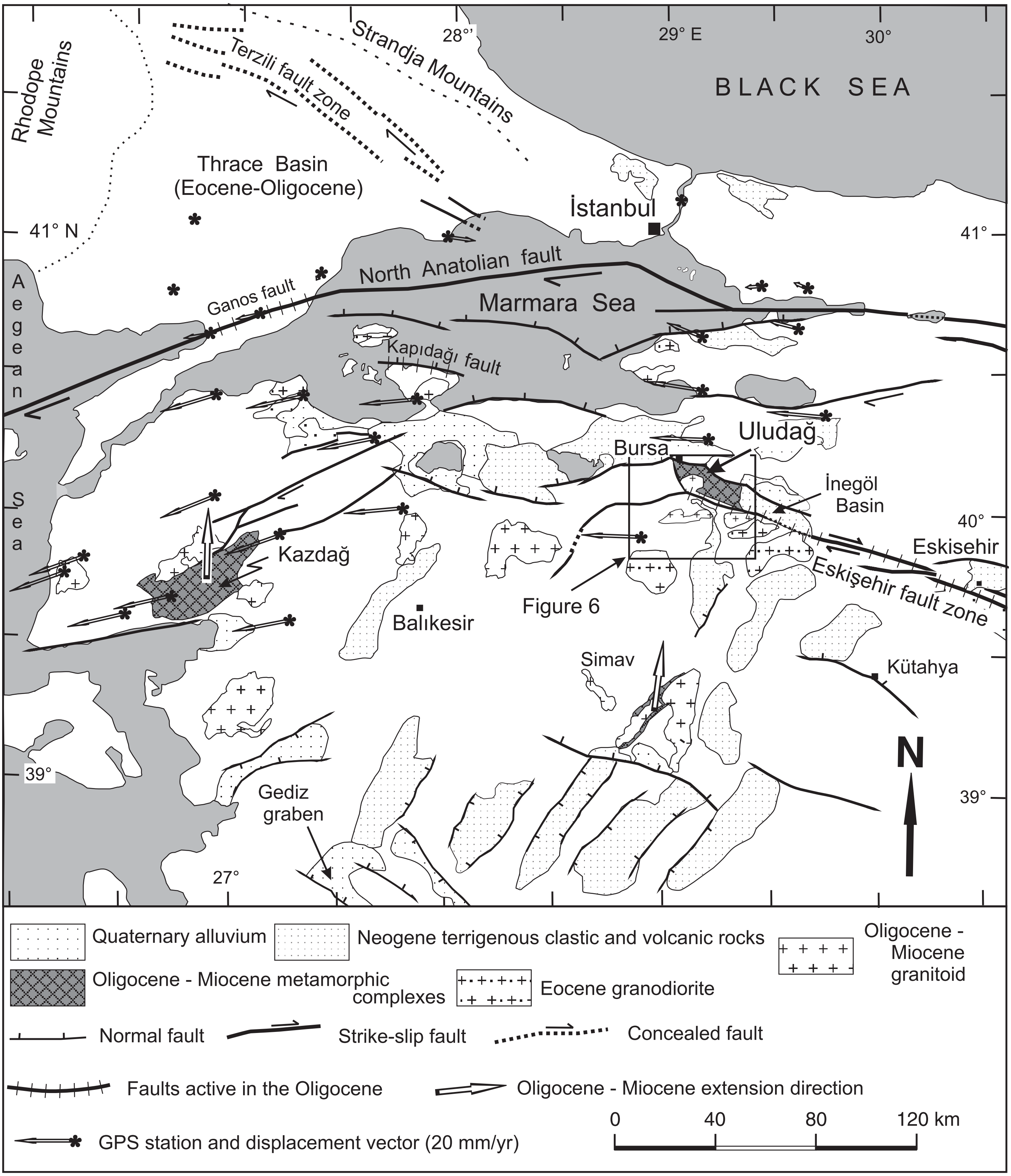

Figure 2. Tectonic map of northwestern Turkey showing the major Neogene basins, alluvial plains, and post-Miocene faults. GPS—global positioning system.

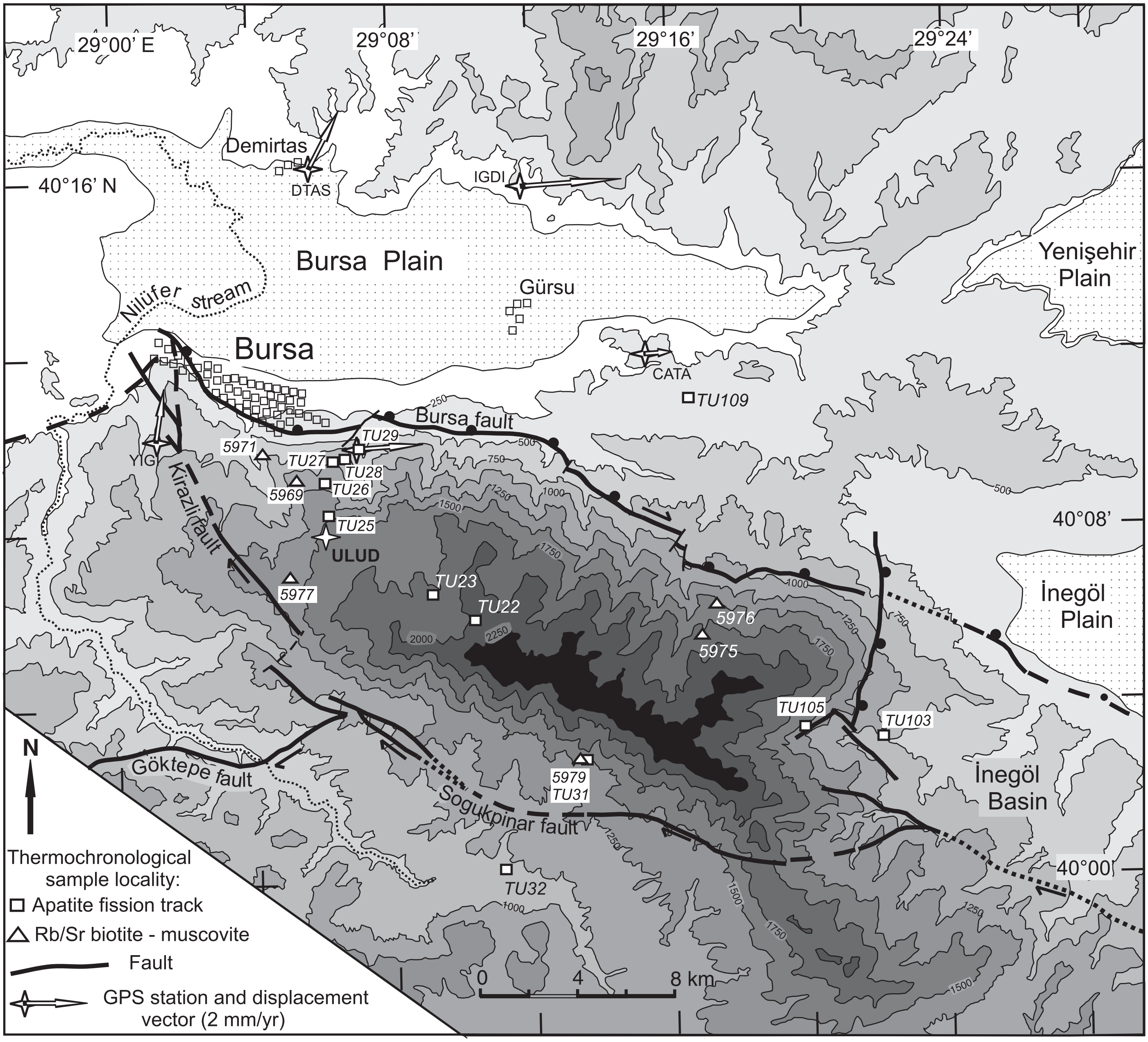

Figure 3. Topography of the Uludağ range, major faults, and the location of geochronological samples. Global positioning system (GPS) velocities are shown with respect to the station ULUD using the data set of Straub (1996). CATA—Çataltepe; DTAS—Demirtaş; IGDI—İğdir; ULUD—Uludağ.

by steeply dipping fault scarps (Fig. 3). The range is bounded in the north by the active Bursa fault, which probably ruptured during the April 11, 1855 Bursa earthquake (M ≈ 6.6; Sandison, 1855). The fault plane, as observed at a few localities, dips at 25°N to 50°N; slickensides indicate a normal sense of motion with a right-lateral strike-slip component (Imbach, 1992; Yıldırım et al., 2005). Large alluvial fans extend from the Bursa fault toward the Bursa Plain. GPS data are available from stations around Bursa (Straub, 1996). These data, recalculated with respect to a station near the summit of Uludağ (ULUD), indicate right-lateral transtensional sense of movement along the Bursa fault at rates between 1 and 2 mm/yr (Fig. 3).

The Uludağ range is bounded in the south by the subvertical Soğukpınar strike-slip fault, which forms a prominent morphological feature. However, there is little evidence for Quaternary fault activity south of Uludağ. The Soğukpınar fault constitutes the westernmost segment of the Eskişehir fault, a broad fault zone that is more than 225 km long and 15 km wide, consisting of 5–25-km-long en echelon faults; it extends east-southeast (109°) from Uludağ to the Sivrihisar region (Figs. 1 and 2; Şengör et al., 1985; Şaroğlu et al., 1992; Altunel and Barka, 1998; Bozkurt, 2001; Yaltırak, 2002). Koçyiğit (2005) and Özsayın and Dirik (2007) extended the Eskişehir fault zone farther east to the Salt Lake in central Anatolia and joined it to the right-lateral strike-slip faults west of the lake (Çemen et al., 1999), giving a total length of 470 km. At least some segments of the Eskişehir fault are active, as shown by the 20 February 1956 Eskişehir earthquake (M_S = 6.4), which had an epicenter north of Eskişehir and a focal mechanism solution indicating normal faulting with minor right-lateral strike-sip (McKenzie, 1972). The sense of slip in the Eskişehir fault zone, as measured on exhumed fault planes, is also right-lateral transtensional (Ocakoğlu, 2007; Tokay and Altunel, 2005).

The Eskişehir fault marks approximately the northeastern limit of the Aegean extensional system (Barka et al., 1995; Koçyiğit, 2005). Along most of its length, it also corresponds to the İzmir-Ankara suture, a profound geological discontinuity between the Pontides to the north and the Anatolide-Taurides to the south (e.g., Okay and Tüysüz, 1999). A sharp change in the Bouguer gravity anomaly across the Eskişehir fault indicates a reduced crustal thickness north of the fault (Fig. 4; Ateş et al., 1999; see also http://www.mta.gov.tr/english/harita/bouger.html). The association of the Eskişehir fault with long-wavelength Bouguer gravity anomalies indicates a deep crustal discontinuity.

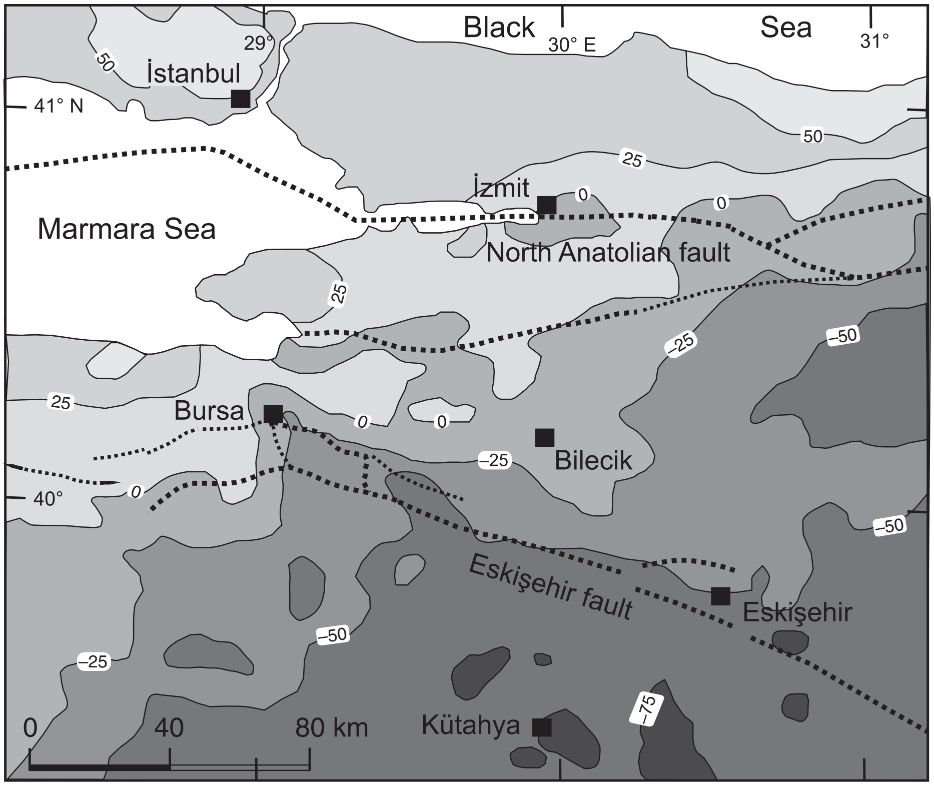

Figure 4. Bouguer gravity anomaly map of northwestern Turkey. The contours are in milligals (based on http://www.mta.gov.tr/english/harita/bouger.html). The major faults are shown by dotted lines.

The Uludağ Massif is located on the Bursa syntaxis where the Eskişehir fault terminates and the İzmir-Ankara suture makes an ~80° counterclockwise bend (Fig. 1; Okay and Tüysüz, 1999). Pre-Miocene sequences on both sides of the Eskişehir fault (Izmir-Ankara suture) are different and cannot be correlated (Fig. 5). The high-grade metamorphic rocks of the Uludağ Group, pierced by Oligocene granite, constitute the lowermost tectonic unit north of the suture. The Uludağ Massif is made up of both the Uludağ Group and the Oligocene granites. The Uludağ Group is tectonically overlain by the Triassic Karakaya Complex, which is interpreted as Paleo-Tethyan subduction-accretion units, and which are in turn unconformably overlain by little-deformed Jurassic-Cretaceous sandstones and limestones (Figs. 5A and 6). The Tavşanlı zone of the Anatolide-Taurides crops out south of the İzmir-Ankara suture. Here, the lowest exposed unit is a coherent blueschist sequence with Late Cretaceous (ca. 80 Ma) metamorphic ages (Okay et al., 1998; Sherlock et al., 1999). The blueschists are tectonically overlain by an accretionary complex and by large slabs of Cretaceous ophiolite (Figs. 5B and 6). Eocene granodiorites cut the blueschists as well as the overlying accretionary complex and ophiolite. Miocene terrigenous deposits make up the oldest formation, which extends across the suture indiscriminately.

THE MIDCRUSTAL SHEAR ZONE—THE ULUDAĞ MASSIF

The Uludağ Group forms a rhomb-shaped, fault-bounded elongate body of gneiss and marble, ~32 km long and ~12 km wide (Fig. 6; Ketin, 1947). It is bounded on the northeast and west by the brittle Bursa and Kirazlı faults, respectively. Locally, there are tectonic slivers of serpentinite along the Bursa fault (e.g., south of Alaçam in Fig. 6; Ketin, 1984). Although the Kirazlı fault is very poorly exposed, the orientation of foliation in its vicinity suggests that it dips steeply to the southwest. It is not active and is cut by the Bursa fault (Figs. 6 and 7A). Toward the northwest, the Uludağ Group gradually tapers off under the tectonic cover of the Karakaya Complex; in the southeast, it is downfaulted by a north-south–trending normal fault.

Stratigraphically, the age of the Uludağ Group is poorly constrained. Poorly preserved solitary corals in the marbles suggest a post-Ordovician

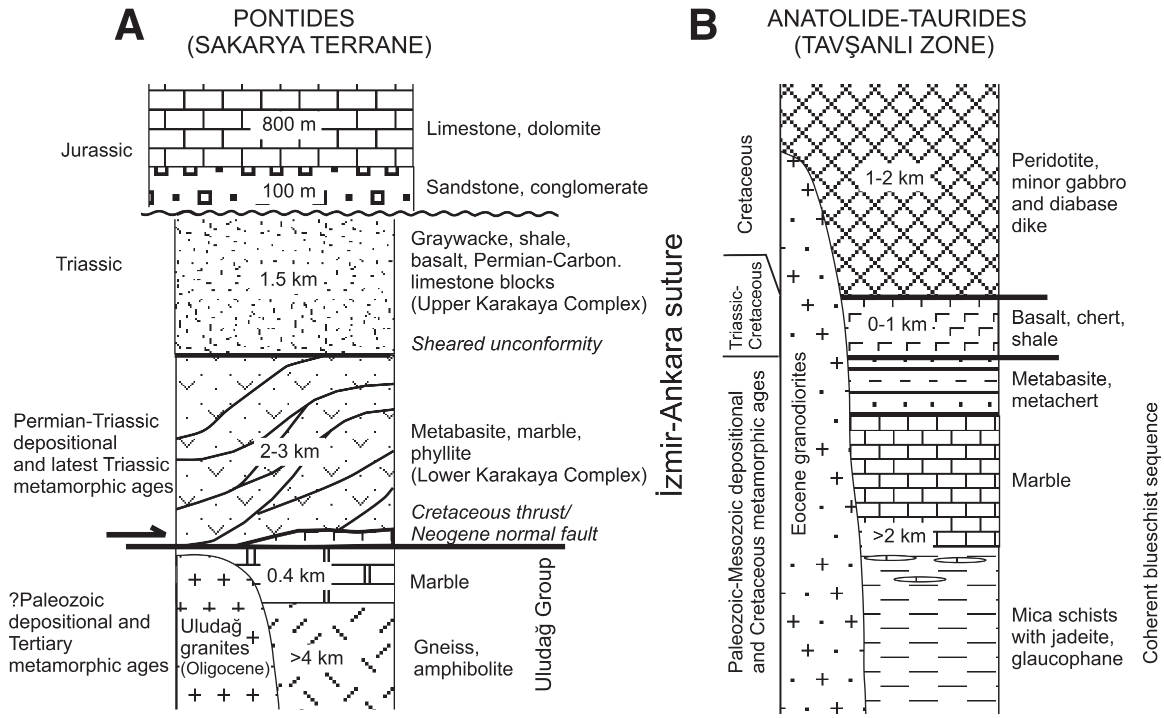

Figure 5. Synthetic stratigraphic sections north and south of the Eskişehir fault (Izmir-Ankara suture) in the Bursa region (modified from Okay and Satır, 2006).

protolith age (Imbach, 1992; Okay, personal observation at UTM 6′73″900/44′47″850); the age of the gneisses is not known. The oldest sediments, which lie unconformably over the metamorphic rocks, are Quaternary alluvium and scree. However, clasts derived from the Uludağ Group are found in the Miocene İnegöl Basin in the east. The Uludağ Group is also cut by the Central and South Uludağ granites, which have Oligocene ages. Preliminary single-zircon step-wise Pb-evaporation ages from the Uludağ gneisses range from 500 Ma to 180 Ma, with a cluster between 300 Ma and 200 Ma (M. Satır, 2006, personal commun.).

The gneisses of the Uludağ Group form an ~4-km-thick sequence made up predominantly of quartzo-feldspathic rocks. A pervasive millimeter-thick color banding defined by variations in the mineral modes, and an equally pervasive mineral stretching lineation are ubiquitous (Figs. 8A and 8B). A granitic origin for the quartzo-feldspathic gneiss is suggested by the homogeneous lithology and by the absence of metasedimentary interlayers. Syn- to late-tectonic aplitic to pegmatitic veins, millimeter to meter in thickness, are common and make up ~15% of the outcrops. The veins strike generally subparallel to the gneissic foliation and frequently exhibit ductile to semibrittle deformation (Figs. 8A and 8D). Hornblende-gneiss and amphibolite occur as rare bands or elongate lenses, a few to ten meters in width, intercalated with the quartzo-feldspathic gneiss. The finely banded marble unit, up to 400 m in thickness, forms two semicontinuous bands along the northern rim and in the center of the Uludağ Massif (Figs. 6 and 7C). Individual marble layers also occur within the gneisses close to the main marble contact.

Structure

The gneisses show a strong high-temperature foliation and compositional banding, which are variously overprinted by a subparallel lower-temperature mylonitic fabric defined by quartz ribbon, oblique quartz fabric, strained and rotated feldspar porphyroblasts, and mica fish. The foliation in the gneisses and amphibolites strikes ESE (~114°), parallel to the mountain range, and dips north to northeast at an average angle of ~35° (Fig. 9A). The dips are subvertical south of the synkinematic South Uludağ granite. The strike of the banding is consistent except at the margins of the Central Uludağ pluton. A subhorizontal mineral stretching lineation defined by the subparallel alignment of hornblende, biotite, and felsic minerals is pervasive in the central part of the Uludağ Group (Fig. 8B). The lineation becomes weaker toward the margins of the Uludağ Massif, where it is overprinted by downdip lineation related to the later normal faulting. The gently dipping lineation in the gneisses trends ~114° (Fig. 9B). Folds are rare; a high concentration of close folds is observed only at a few localities in the gneisses. The fold axis trends parallel to the mineral lineation, which is typical for highly strained rocks. Boudinaged structures are commonly found in the aplitic veins in gneiss and the dolomitic bands in marble. Low-temperature structures, such as brittle microfaults, are rare.

Macroscopic shear sense indicators are widespread in the gneisses and in the marbles, and they consistently indicate a right-lateral motion. The thin dolomite layers in the marbles and the synkinematic aplite veins in the gneisses especially are stretched and sheared parallel to the layering, producing asymmetric σ-type boudins and pinch-and-swell structures that indicate a right-lateral shear sense (Figs. 8C and 8D). Asymmetric tails of feldspar porphyroclasts in the gneisses and C′-type shear bands in the micaceous metamorphic rocks also consistently indicate right-lateral shear (Fig. 8D).

Petrology and Pressure-Temperature Conditions

The gneisses range from biotite gneiss to hornblende-biotite gneiss and grade locally into amphibolite, with a decrease in the quartz content. Biotite, muscovite, and chlorite occur

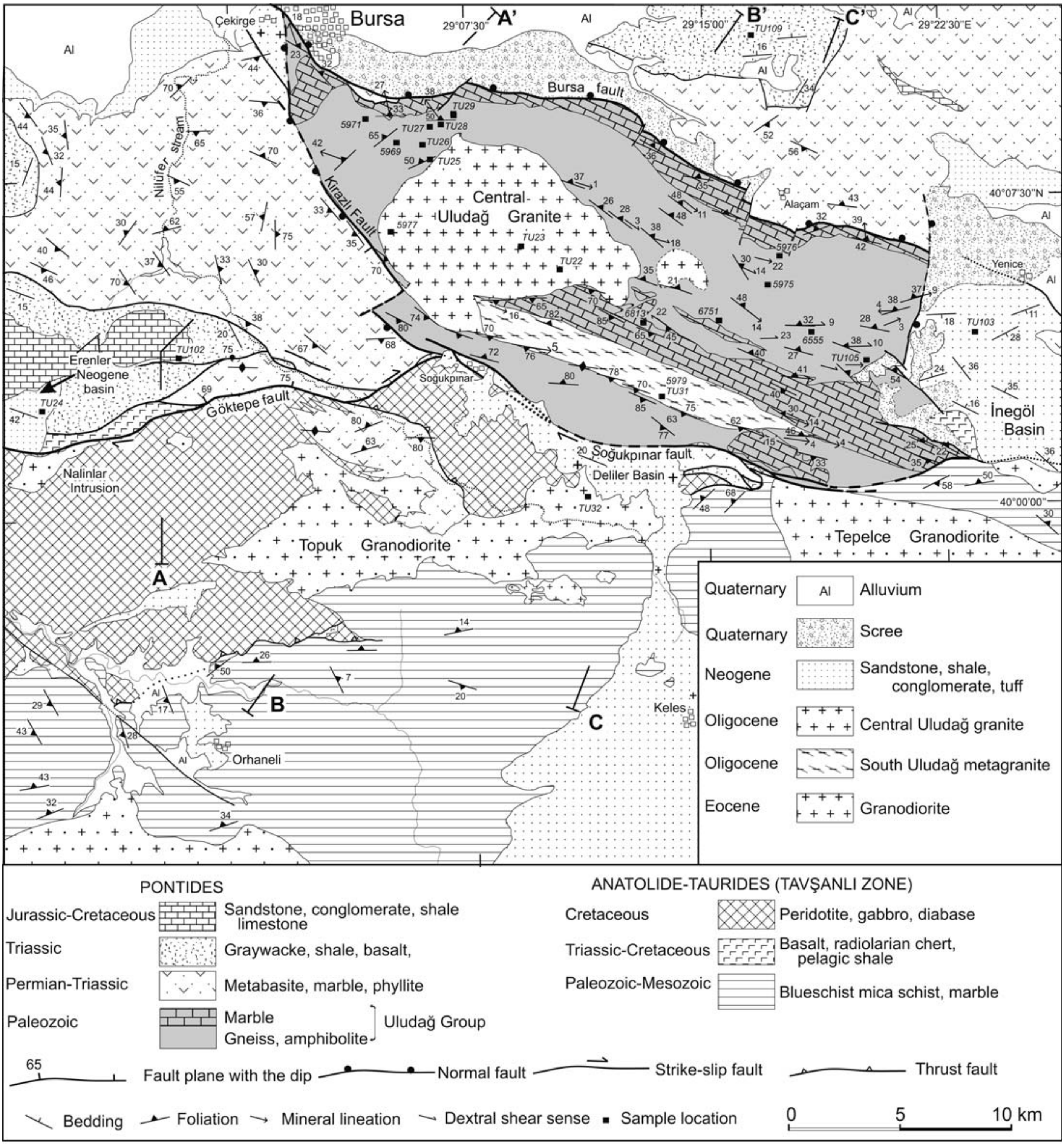

Figure 6. Geological map of the Uludağ region (based on Ketin, 1947; Lisenbee, 1971; Okay et al., 1998; this study). For location, see Figure 2.

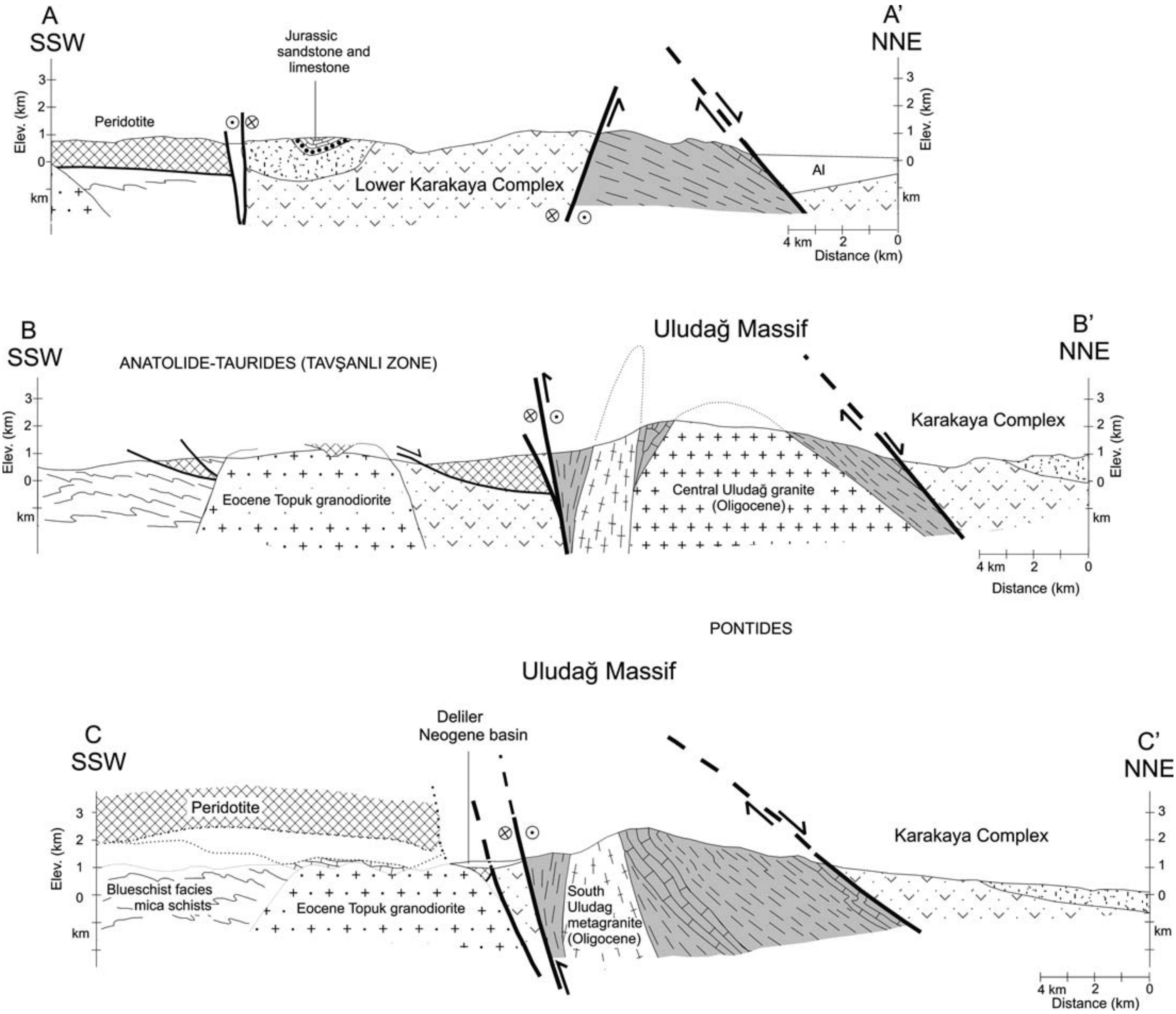

Figure 7. Cross sections from the Uludağ region. For locations of the sections, see Figure 6.

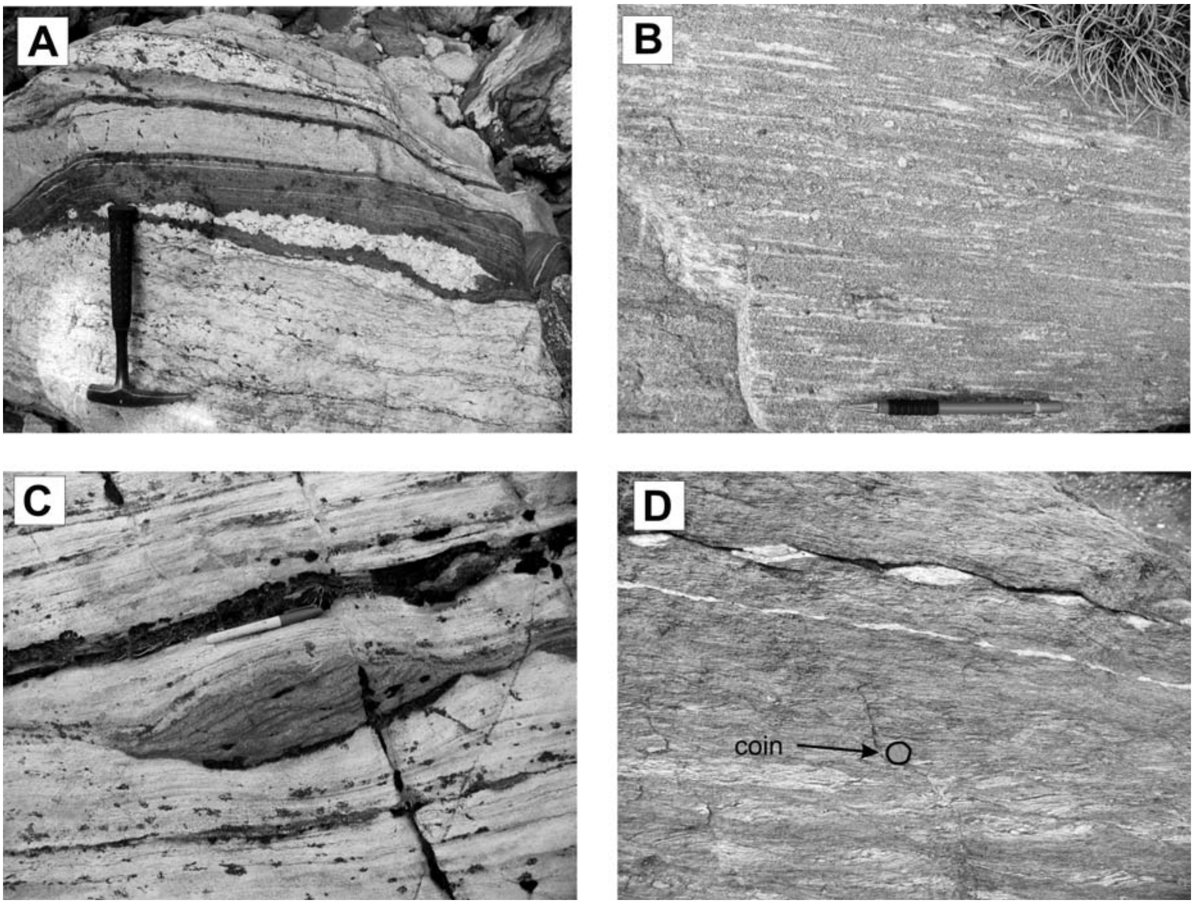

Figure 8. Field photographs from the Uludağ Group. (A) Banded quartzo-feldspathic gneiss cut by synkinematic pegmatitic veins. (B) Subhorizontal mylonitic mineral lineation on a foliation plane in gneiss. (C) Boudinaged and rotated dolomite layer in marble showing a right-lateral shear sense. (D) Synkinematic aplitic veins and weakly developed C′-type shear bands indicating a right-lateral shear sense.

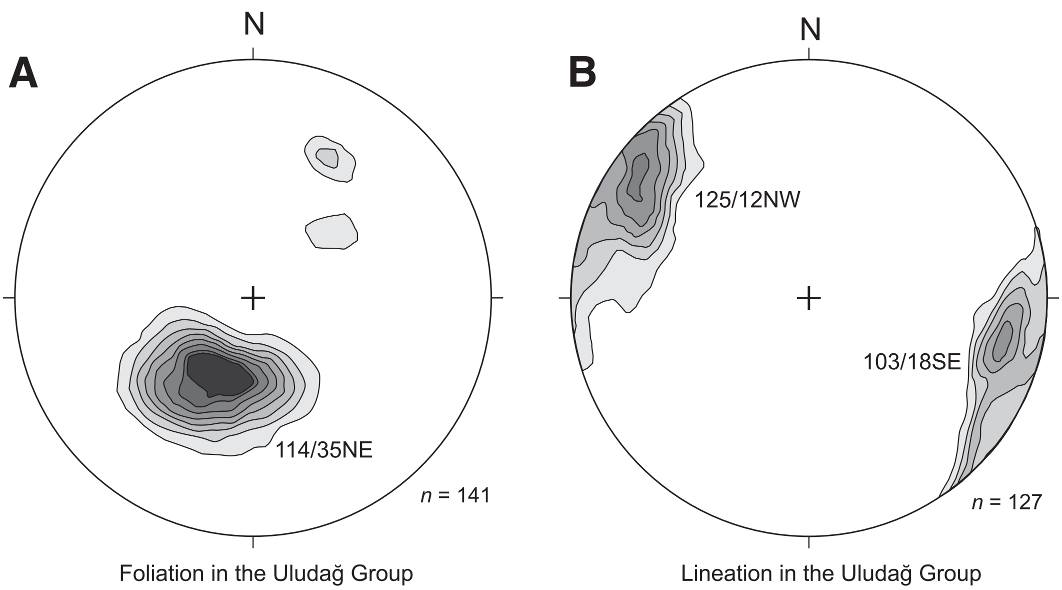

Figure 9. Equal-area, lower-hemisphere projection of structural data from the Uludağ Group. Contours are at 2%, 4%, 6%, 8%, 10%, 12%, 14%, and 15% for one-percent area for the foliation, and at 2%, 3%, 4%, 5%, 6%, and 7% for one-percent area for the lineation.

in millimeter- to centimeter-thick bands alternating with more felsic layers. The Uludağ Group has undergone amphibolite-facies metamorphism, and there is no measurable change in the metamorphic grade across the area. The common mineral assemblage in the gneisses is quartz + plagioclase + biotite + hornblende + muscovite ± chlorite ± garnet ± K-feldspar ± ilmenite. Quartz, feldspar, biotite, hornblende, and muscovite are the major minerals that form the medium-sized grains, 0.2–0.5 mm across. Garnet is rare and occurs as a matrix mineral and/or as poikilitic porphyroblasts, up to 2 cm across. In amphibolites, garnet porphyroblasts are partly to completely replaced by hornblende and plagioclase. Dark bluish green hornblende forms prismatic grains, up to 2 mm long, and is associated with biotite. Plagioclase commonly forms microporphyroblasts with quartz and biotite inclusions.

Two samples of biotite-gneiss, two of hornblende-gneiss, and one amphibolite were analyzed with a Camebax SX-51 electron microprobe at the University of Heidelberg, Germany, to constrain the pressure-temperature (*P-T*) evolution. The estimated modes of the analyzed samples are given in Table 1, and the representative mineral compositions are given in Table 2. No previous petrologic data are available from the Uludağ Massif.

TABLE 1. MODES OF THE ANALYZED ULUDAĞ ROCKS

Sample	Garnet-biotite gneiss		Hornblende gneiss		Amphibolite
	6555	6763	6751	6811	6806
Quartz	40	35	13	11	4
Plagioclase	7	26	33	22	37
K-feldspar	-	6	-	-	3
Al_2SiO_5	tr	-	-	tr	-
Garnet	9	2	12	17	19
Hornblende	-	-	9	21	28
Biotite	6	23	23	23	3
Muscovite	31	7	4	-	-
Chlorite	4	1	3	3	tr
Epidote	1	-	tr	-	1
Rutile	tr	-	tr	tr	tr
Titanite	-	-	tr	-	tr
Ilmenite	2	-	2	2	3
Magnetite	-	-	1	-	2
Hematite	-	-	-	1	-
Pyrite	-	-	tr	-	-
Apatite	tr	tr	-	-	tr

Note: tr—trace, less than 0.5%.

Mineral Chemistry

Garnets are almandine-pyrope-grossular-spessartine solid solutions, and they display a strong compositional variation from sample to sample, reflecting different initial bulk compositions (Fig. 10A; Table 2). They generally show growth zoning, with a decrease in the spessartine and almandine contents and increase in pyrope toward the rim, while the grossular content stays relatively constant (Table 2). Locally, there is a reversal in growth zoning in the outermost rim domain (<0.3 mm) ascribed to the retrograde net-transfer reactions and Fe-Mg exchange during temperature

TABLE 2. REPRESENTATIVE MINERAL COMPOSITIONS FROM THE ULUDAĞ GROUP

	Garnet-biotite gneiss 6763					Garnet-biotite gneiss 6555					Hornblende-gneiss 6751					
	garnet rim	biotite	musc.	plag.	ilmenite	Al_2SiO_5 inc.	garnet rim	biotite	musc.	plag.	garnet core	garnet rim	hornbl.	plag.	biotite	musc.
SiO_2	36.71	33.01	46.30	62.49	0.07	37.99	37.12	35.05	46.13	60.45	37.10	38.14	44.61	59.47	36.63	46.89
TiO_2	0.02	1.70	0.72	0.00	49.31	0.00	0.03	1.80	0.80	0.00	0.00	0.00	0.64	0.00	2.12	1.06
Al_2O_3	20.39	15.33	30.70	24.49	0.00	62.12	20.60	17.56	33.56	25.95	20.98	21.07	11.06	27.37	16.21	31.74
Cr_2O_3	0.00	0.02	0.06	0.00	0.00	0.00	0.04	0.09	0.03	0.00	0.04	0.00	0.01	0.00	0.02	0.00
FeO	27.35	23.34	4.84	0.14	39.67	1.57	31.02	18.99	2.08	0.10	32.00	24.21	17.07	0.21	17.18	3.84
MnO	10.66	0.63	0.05	0.00	8.71	0.04	6.60	0.22	0.02	0.00	4.70	7.27	0.71	0.00	0.63	0.00
MgO	1.99	7.28	0.97	0.00	0.03	0.04	2.42	9.96	0.59	0.00	2.36	3.62	10.38	0.00	12.45	0.99
CaO	2.81	0.00	0.00	5.27	0.01	0.05	2.14	0.00	0.02	6.73	3.78	7.07	11.78	8.38	0.01	0.06
Na_2O	0.00	0.07	0.40	8.88	0.02	0.00	0.04	0.14	0.69	8.17	0.00	0.00	1.11	7.29	0.11	0.36
K_2O	0.07	9.45	10.50	0.23	0.16	0.01	0.01	9.01	9.66	0.08	0.02	0.00	0.44	0.09	9.73	10.14
Total	100.00	90.82	94.54	101.49	97.97	101.82	100.02	92.81	93.58	101.47	100.98	101.38	97.82	102.80	95.07	95.09
Mineral formula on the basis of																
	12 O	11 O	11 O	8 O	3 O	5 O	12 O	11 O	11 O	8 O	12 O	12 O	23 O	8 O	11 O	11 O
Si	2.988	2.737	3.170	2.734	0.002	1.013	3.005	2.739	3.126	2.656	2.975	2.993	6.554	2.590	2.781	3.163
Ti	0.001	0.106	0.037	0.000	0.951	0.000	0.002	0.106	0.041	0.000	0.000	0.000	0.071	0.000	0.121	0.054
Al	1.956	1.497	2.478	1.263	0.000	1.952	1.965	1.618	2.681	1.344	1.982	1.949	1.916	1.405	1.451	2.523
Cr	0.000	0.001	0.003	0.000	0.000	0.000	0.003	0.005	0.002	0.000	0.002	0.000	0.001	0.000	0.001	0.000
Fe^{3+}	0.044			0.005		0.030	0.030			0.003	0.041	0.058	0.660	0.008		
Fe^{2+}	1.807	1.618	0.277		0.850		2.070	1.241	0.118		2.105	1.531	1.438		1.091	0.217
Mn	0.735	0.044	0.003	0.000	0.189	0.001	0.452	0.015	0.001	0.000	0.319	0.483	0.088	0.000	0.040	0.000
Mg	0.242	0.900	0.099	0.000	0.001	0.002	0.292	1.160	0.060	0.000	0.282	0.424	2.272	0.000	1.409	0.100
Ca	0.245	0.000	0.000	0.247	0.000	0.001	0.186	0.000	0.001	0.317	0.325	0.594	1.884	0.391	0.001	0.004
Na	0.000	0.011	0.053	0.753	0.001	0.000	0.006	0.020	0.091	0.696	0.000	0.000	0.322	0.616	0.015	0.047
K	0.007	0.999	0.918	0.013	0.005	0.000	0.001	0.899	0.835	0.005	0.002	0.000	0.085	0.005	0.942	0.872
	8.026	7.913	7.037			2.999	8.012	7.803	6.955	5.020	8.034	8.033	15.290	5.014	7.851	6.981
Activities at 670 °C and 7 kbar																
	0.19	0.19	mu	an 0.35	ilm		0.31	phl	mu	an 0.46	alm 0.30	0.11	tr	an 0.56	phl	mu
alm			0.55		0.71	alm		0.051	0.67				0.041		0.084	0.57
	0.00081	0.00079	pa	ab 0.75	hem 0.003		0.00132	ann	pa	ab 0.69	py	0.0063	pg 0.08	ab 0.62	ann	pa
pyr			0.238			pyr		0.056	0.477		0.0015				0.040	0.238
	0.00058	0.00057	cel				0.0003	east	cel		gr	0.0097			east	cel
gross			0.028			gross		0.041	0.016		0.0016				0.046	0.027

Note: The Fe_3+ in the amphibole was calculated assuming 23 oxygens in the structural formula and Si + Ti + Al + Fe_3+ + Fe_2+ + Mg + Mn = 13.0.

Abbreviations: inc.—inclusion; musc.—muscovite; plag.—plagioclase; hornbl.—hornblende; O—oxygens; ab—albite; alm—almandine; an—anorthite; ann—annite; cel—celadonite; east—eastonite; gr—grossular; mu—muscovite; pa—paragonite; pg—pargasite; phl—phlogopite; pyr—pyrope; tr—tremolite.

Operating parameters for the electron microprobe were 15 kV accelerating voltage, 20 nA beam current, ~1 μm beam size (for feldspars 10 μm) and 10 s counting time for all elements.

decrease. Calcic amphiboles from the gneisses and amphibolites are magnesio-hornblende to tschermakite (Fig. 10B). The Mg numbers (Mg/[Mg + Fe^{2+}]) of the analyzed biotites show a wide range between 0.30 and 0.60, but they correlate positively with the Mg numbers of the coexisting garnets (0.09–0.36) (Fig. 10C). Muscovite is characterized by Si cation values of 3.06–3.21 in the 11 oxygen formula unit. Muscovite inclusions in garnets display higher TiO_2 concentrations (up to 1.5 wt%). Plagioclase is mostly oligoclase to andesine and seldom labradorite (Fig. 10F). In some samples, the compositional variation is quite large (up to 40 mol%). Two of the samples (6806 and 6763) contain K-feldspar, which is essentially an end-member composition with minor albite (<8 mol%) and anorthite (<1 mol%) components. The wide range in the mineral compositions within single rock samples (Fig. 10) is compatible with continuous and incomplete reequilibration in a shear zone.

Geothermobarometry

The low-variance matrix assemblage during peak metamorphic conditions is inferred to be hornblende + garnet + plagioclase + biotite + muscovite + quartz + ilmenite in the hornblende-gneiss and amphibolite, and garnet + plagioclase + biotite + muscovite + quartz in the biotite-gneiss. The *P-T* conditions were estimated from these mineral assemblages using both conventional geothermobarometers and the THERMOCALC program of Powell and Holland (1988). For the THERMOCALC program, the thermodynamic data set of Holland and Powell (1998) was used. The mineral activities were determined using the AX program (wwww.esc.cam.ac.uk/astaff/holland) from the representative mineral compositions listed in Table 2. THERMOCALC gives relatively precise *P-T* estimates of 640 ± 30 °C and 6.2 ± 1.1 kbar for the garnet-biotite gneisses (6555 and 6763) based largely on equilibria between garnet, biotite, muscovite, plagioclase, and quartz (Fig. 11). The error bars are larger in the hornblende-gneiss and amphibolite samples, which yield temperature and pressure ranges of 625–750 °C and 6–9 kbar, respectively.

Hornblende-plagioclase thermometry (Holland and Blundy, 1994) together with garnet-hornblende-plagioclase-quartz barometry (Kohn and Spear, 1990) yields 690 ± 60 °C and 6.3 ± 1.3 kbar for the adjoining plagioclase, hornblende, and garnet assemblages (Fig. 11). Garnet-biotite thermometry of Ferry and Spear (1978) together with garnet-biotite-plagioclase-quartz barometry (Hoisch, 1990, 1991) yield 710 ± 35 °C and 6.5 ± 0.7 kbar, using garnet core and matrix biotite and plagioclase compositions from the garnet-biotite gneiss 6555. The presence of muscovite and quartz and absence of Al_2SiO_5 + K-feldspar indicate that the peak *P-T* conditions did not exceed muscovite + quartz stability (Fig. 11). The peak *P-T* estimates on the basis of conventional geothermobarometry and THERMOCALC are 670 ± 40 °C and 7.0 ± 1.0 kbar.

The growth zoning in garnet observed in the amphibolite and hornblende gneisses indicates that the inclusion assemblages together with the garnet composition can be used to place *P-T* constraints on the early evolution of the rocks. The inclusions in garnet include Al_2SiO_5, quartz, muscovite, chlorite, biotite, quartz, hornblende, rutile, and ilmenite. The very fine grain size of Al_2SiO_5 mineral does not allow optical identification. Temperatures can be obtained by the Fe-Mg partitioning between hornblende inclusions and garnet in contact with the inclusions, under the assumption that no Fe-Mg exchange

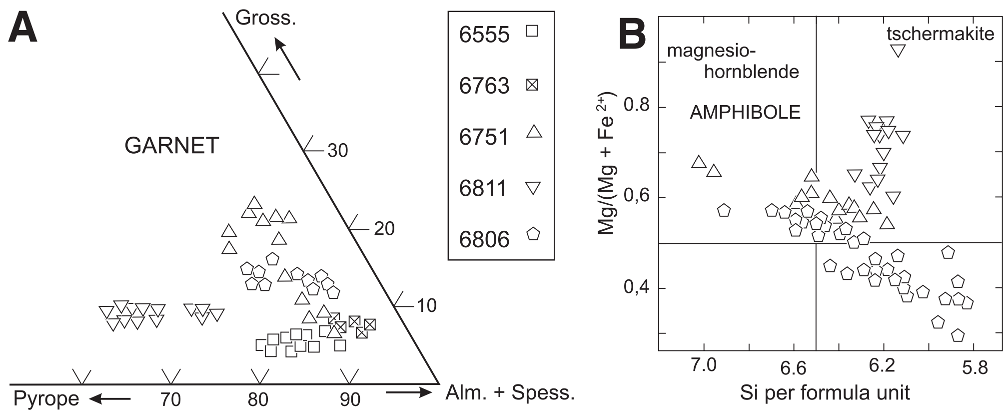

Figure 10. Mineral compositions from the Uludağ gneiss and amphibolite: (A) garnet compositions plotted on the grossular (Gross), pyrope, and almandine + spessartine (Alm + Spess) ternary diagram. (B) Calcic amphibole, (C) biotite, (D) muscovite, (E) chlorite, and (F) plagioclase compositions. Each point represents a single analysis.

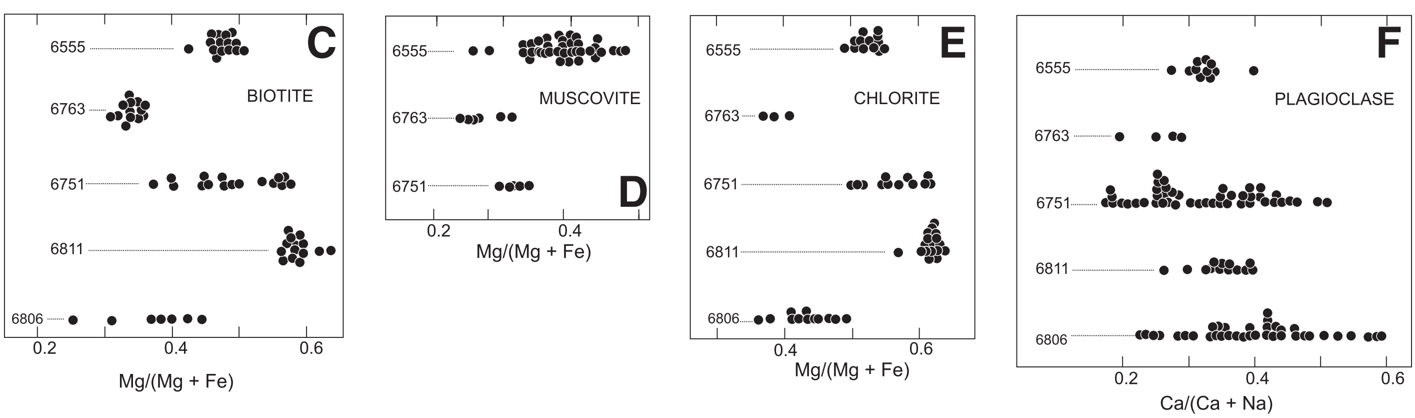

takes place between garnet and hornblende. Garnet-hornblende thermometry after the formulation of Graham and Powell (1984) yields temperatures of 575 ± 25 °C (Fig. 11).

Pressures can be estimated using the garnet-rutile-ilmenite-plagioclase-silica (GRIPS), garnet-rutile-aluminium-silicate-ilmenite (GRAIL), and garnet-aluminium-silicate-silica-plagioclase (GASP) equilibria:

2 almandine + grossular + 6 rutile = 6 ilmenite + 3 anorthite + 3 quartz;

almandine + 3 rutile = 3 ilmenite + Al_2SiO_5 + 2 quartz;

3 anorthite = grossular + 2 Al_2SiO_5 + quartz.

These equilibria indicate pressures of 7.6 ± 0.6 kbar, 6.5 ± 0.5 kbar, and 6.7 ± 0.9 kbar, respectively (Bohlen and Liotta, 1986; Bohlen et al., 1983; Koziol and Newton, 1988). To summarize, garnet growth probably occurred at temperatures of 575 ± 25 °C and pressures of 6.9 ± 1.0 kbar, suggesting isobaric heating during the evolution of the Uludağ Group.

The retrograde assemblages are defined by biotite + plagioclase + quartz + chlorite + muscovite + epidote + ilmenite + magnetite. This assemblage is characteristic of epidote amphibolite-facies conditions. *P-T* conditions of the retrograde stage are not well constrained.

Syn- and Postkinematic Oligocene Granites

Two intrusive granitic bodies of similar age but with different textural features are present in the Uludağ Massif: the strongly anisotropic sheet-like South Uludağ metagranite and the undeformed dome-shaped Central Uludağ granite.

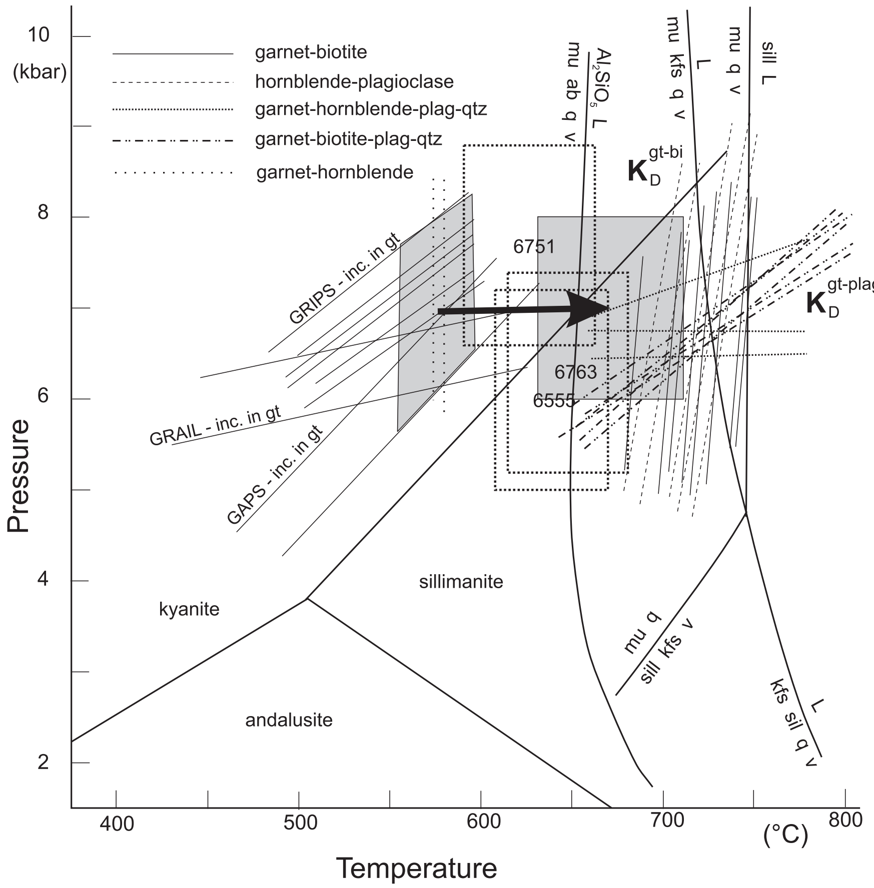

Figure 11. Pressure-temperature (*P-T*) diagram showing the equilibria relevant for the estimation of the *P-T* conditions of the Uludağ Group. End-member reactions are from THERMOCALC; liquidus reactions are from Spear et al. (1999). The dotted rectangles indicate the peak *P-T* conditions estimated using THERMOCALC for the samples shown. The arrow indicates inferred prograde metamorphic evolution of the Uludağ Group. Abbreviations: inc.—inclusions; ab—albite; gt—garnet; ksp—K-feldspar; L—silicate liquid; mic—microcline; mu—muscovite; phl—phlogopite; q—quartz; sill—sillimanite; v—H_2O.

South Uludağ Metagranite—Synkinematic Intrusion

The South Uludağ metagranite is a subvertical, sheet-like intrusion with a length of 17 km and a thickness of only ~1.5 km. It strikes ESE (110°) and pinches out toward the southeast (Fig. 6). It is intrusive into the Uludağ Group along its northern and southern contacts and is intruded by the Central Uludağ Granite. Contact metamorphism is not observed, implying that the gneisses were still at elevated temperature conditions during the intrusion. The South Uludağ metagranite is a fine-grained, leucocratic intrusion, which consists chiefly of quartz and feldspar with minor muscovite and biotite. It shows a high-temperature solid-state foliation and lineation defined by biotite, muscovite, quartz, and subparallel alignment of feldspar porphyroclasts. Quartz has recrystallized to finer-grained aggregates that are 0.1–0.2 mm across and elongated subparallel to the foliation. Feldspar largely retains the igneous crystal form, forming 1–2-mm-long and 0.5-mm-wide coarse grains, without any cataclasis or recrystallization. Quartz and feldspar fabrics suggest deformation temperatures of ~400 °C (e.g., Passchier and Trouw, 1998, p. 48). The high-temperature foliation is cut discordantly by aplitic veins. The sheet-like geometry of the South Uludağ metagranite, with its long axis parallel to the strike of the dominant foliation, its asymmetric tail, and the solid-state/crystal-plastic strain fabrics, indicates that it is a synkinematic pluton emplaced during the right-lateral shear-zone activity. Contemporaneous high-temperature shear and acidic magmatic activity have also been described from other strike-slip shear zones (e.g., Schärer et al., 1994; Anczkiewicz et al., 2007).

Central Uludağ Granite—Postkinematic Pluton

The two-mica Central Uludağ granite crops out over an elliptical area of 11 km by 6.5 km (Fig. 6). It has outward-dipping intrusive contacts with the Uludağ Group and cuts the fabric in the gneisses (Fig. 7; Ketin, 1947). A skarn complex with economic wolframite deposits has formed along the granite-marble contact (van der Kaaden, 1958). The Central Uludağ granite is a homogeneous, fine- to medium-grained granite of quartz, plagioclase, K-feldspar, biotite, and muscovite (Ketin, 1947; Öztunalı, 1973). Geochemically it is peraluminous and highly potassic.

The Uludağ granites are located at the northeastern margin of the large Oligocene-Miocene magmatic province of northwest Turkey, which is characterized by more than ten granitoid intrusions and voluminous volcanic and volcaniclastic rocks (Fig. 2; e.g., Seyitoğlu and Scott, 1992; Delaloye and Bingöl, 2000; Aldanmaz et al., 2000). With the exception of the Uludağ granites, all the other Oligocene-Miocene plutons are metaluminous and are generally represented by hornblende-biotite–bearing granodiorites (e.g., Karacık and Yılmaz, 1998; Yılmaz et al., 2001). The peraluminous geochemistry and the presence of muscovite in the Uludağ granites indicate an important crustal component in their genesis.

Thermochronology of the Uludağ Massif

We used U/Pb, Rb/Sr, and apatite fission-track (AFT) geochronological methods to constrain the Tertiary evolution of the Uludağ Massif. Sample preparation and analysis for the U/Pb and Rb/Sr methods followed the procedures outlined in Okay and Satır (2006) and those for AFT followed Zattin et al. (2000). The analytical results are given in Tables 3–5, and the locations of the samples are shown on the maps in Figures 3 and 6. For the geological time scale, we used Gradstein et al. (2004).

Rb/Sr and U/Pb Data

Published K-Ar biotite ages from the Central Uludağ granite are 26.8 and 24.7 Ma (Bingöl et al., 1982; Delaloye and Bingöl, 2000), whereas no previous isotopic ages are available for the South Uludağ metagranite. Our new Rb/Sr muscovite and biotite ages from the Central Uludağ granite are 27.5 ± 0.5 Ma and 27.2 ± 0.3 Ma, respectively (Table 3), similar to the K-Ar biotite ages. The coeval muscovite and biotite ages from the Central Uludağ granite indicate fast cooling of the magma and point to a late Oligocene intrusion age. A three-point isochron yields an intrusion age of 27.2 ± 0.2 Ma. Two samples from the South Uludağ metagranite yielded similar Rb/Sr biotite (27.4 Ma and 29.4 Ma) and slightly older muscovite (27.9 Ma and 34.7 Ma) ages (Table 3). Because the South Uludağ metagranite has undergone a high-temperature deformation, we carried out a U/Pb zircon analysis to establish its crystallization age. Four zircons from sample 5979A, which was also dated by Rb/Sr method, gave ages ranging from 30 to 39 Ma (Fig. 12; Table 4). We interpret this spread of ages as prolonged crystallization in a shear zone during the latest Eocene and early Oligocene, probably associated with Pb loss during the intrusion of the Central Uludağ granite. The isotopic ages indicate that the South Uludağ granite crystallized 7–11 m.y. earlier than the Central Uludağ granite; however, they cooled penecontemporaneously to temperatures of ~300 °C.

Four gneiss samples from the Uludağ Group were dated by the Rb/Sr method. Two samples come from the western side of the Uludağ Massif, and two came from the eastern side. They are quartzo-feldspathic gneisses with the mineral assemblage of quartz + plagioclase + biotite ± muscovite ± K-feldspar. The muscovite Rb/Sr age of one of the gneiss samples is 48.7 ± 2.2 Ma. A similar Eocene age of 51.04 ± 0.74 Ma was obtained from coarse muscovites, one centimeter across, in a pegmatite vein in the marble. Biotite Rb/Sr ages from the gneisses are latest Eocene to Oligocene, ranging from 36 to 24 Ma; those from the western part of the Uludağ Massif are older (30.5 ± 0.3 Ma and 35.7 ± 0.4 Ma) than those from the eastern part (24.4 ± 0.2 Ma and 24.5 ± 0.3 Ma) (Table 3). The fast cooling of the Central Uludağ granite, shown by the similar Rb/Sr muscovite and biotite ages (ca. 27 Ma), suggests that ambient temperatures before its intrusion were less than ~300 °C, which is compatible with the early Oligocene (36–31 Ma) biotite Rb/Sr cooling ages. On the other hand, the Rb/Sr biotite ages from the eastern part of the Uludağ Group are difficult to interpret because they are younger than the intrusive Central Uludağ granite. These young ages may be due to shear heating or to the presence of intrusions at depth. Although shear heating is not considered to be a direct cause for metamorphism, nevertheless it can lead to a reopening of the Rb-Sr isotopic system and increases in temperatures of a few hundred degrees (e.g., Leloup et al., 1999).

The closure temperatures of muscovite and biotite for Sr are 500 ± 50 °C and 300 ± 50 °C, respectively (e.g., Jäger et al., 1967; Cliff, 1985). Hence, the Uludağ Group must have cooled from ~500 °C during the Eocene (ca. 50 Ma) to ~300 °C during the Oligocene (ca. 33 Ma), yielding a cooling rate of ~12 °C/m.y. (Fig. 13). The age of peak metamorphism in the Uludağ Group is not known. Extrapolation from the

TABLE 3. Rb/Sr DATA FROM THE ULUDAĞ REGION

Sample	Mineral	Rb (ppm)	Sr (ppm)	$^{87}Rb/^{86}Sr$	$^{87}Sr/^{86}Sr$	Age (Ma)
			Uludağ Gneiss			
5969	rock	38.06	250.5	0.4395	0.705783	
	biotite	320.50	2.939	319.8	0.844250	30.5 ± 0.3
5971	rock	73.77	85.54	2.4959	0.711084	
	biotite	692.10	3.016	685.8	1.046559	35.7 ± 0.4
5975A	rock	58.00	270.8	0.6197	0.707537	
	biotite	609.90	2.725	662.01	0.936396	24.4 ± 0.2
5976	rock	55.91	212.1	0.7629	0.712156	
	biotite	266.00	4.175	185.61	0.776584	24.5 ± 0.3
	muscovite	137.90	38.36	10.416	0.718838	48.7 ± 2.2
			Pegmatite vein			
6813	rock	66.34	202	0.9498	0.705372	
	muscovite	271.50	19.38	40.638	0.734149	51.04 ± 0.74
			Central Uludağ Granite			
5977	rock	122.20	557.1	0.6346	0.706851	
	biotite	791.30	3.732	627.97	0.94885	27.2 ± 0.3
	muscovite	546.90	27.15	58.407	0.729395	27.5 ± 0.5
			South Uludağ Metagranite			
5979A	rock	104.30	399.5	0.7552	0.705933	
	biotite	869.30	6.362	401.34	0.861845	27.4 ± 0.3
	muscovite	547.20	28.74	55.189	0.727508	27.9 ± 0.5
5979B	rock	125.90	393.00	0.9265	0.70575	
	biotite	1233	3.680	1009.10	1.127977	29.5 ± 0.4
	muscovite	673.10	25.40	76.938	0.743182	34.7 ± 0.5

TABLE 4. U-Pb ZIRCON DATA FROM THE SOUTH ULUDAĞ METAGRANITE

Zircons 5979A	Weight (mg)*	$^{206}Pb/^{204}Pb$	U (ppm)	Pb (ppm)	Isotopic ratios				Apparent ages (Ma)		
					$^{208}Pb^*/^{206}Pb^*$	$^{206}Pb/^{238}U$	$^{207}Pb/^{235}U$	$^{207}Pb^*/^{206}Pb^*$	$^{206}Pb^*/^{238}U$	$^{207}Pb^*/^{235}U$	$^{207}Pb^*/^{206}Pb^*$
1	0.0108	637.7	4738	23.0	0.02868	0.00473 ± 04	0.03071 ± 39	0.04711 ± 43	30.4	30.7	54.9
2	0.027	4737	844.3	5.14	0.11205	0.00603 ± 06	0.03892 ± 91	0.04679 ± 99	38.8	38.8	28.9
3	0.017	1004	1004	11.4	0.06924	0.00579 ± 06	0.03657 ± 109	0.04581 ± 125	37.2	36.5	–12.7
4	0.019	1524	2467	12.9	0.06213	0.00529 ± 06	0.03357 ± 84	0.04598 ± 105	34.1	33.5	–3.5

Note: Errors are 2σ absolute uncertainties and refer to the last digits; grain size 80–180 μm; * = radiogenic; mg*—error is up to 10%.

TABLE 5. APATITE FISSION-TRACK DATA FROM THE BURSA REGION

Sample number	Lithology	Rock unit	Height (m)	No. of crystals	Spontaneous		Induced		$P(\chi)^2$	Dosimeter		Age (Ma) ± 1σ	Mean confined track length (μm) ± std. err.	Std. dev.	No. of measured tracks
					ρ_s	N_s	ρ_i	N_i		ρ_d	N_d				
TU22	granite	Central Uludağ granite	2125	20	4.27	254	4.38	2607	85.45	0.96	4564	17.1 ± 1.2	14.66 ± 0.10	1.04	100
TU23	granite	Central Uludağ granite	1780	20	2.99	187	2.18	1359	84.43	1.10	5214	27.7 ± 2.2	-	-	-
TU25	gneiss	Uludağ Group	1560	20	2.57	309	2.36	2841	86.49	1.04	4382	20.7 ± 1.3	14.61 ± 0.13	1.34	100
TU26	gneiss	Uludağ Group	1255	20	0.64	70	0.45	492	99.98	1.11	5233	28.9 ± 3.7	14.83 ± 0.18	0.66	13
TU27	gneiss	Uludağ Group	1035	20	0.80	69	0.80	692	91.82	1.11	5253	20.2 ± 2.6	-	-	-
TU28	gneiss	Uludağ Group	800	20	2.67	289	2.48	2683	39.84	1.06	5040	21.0 ± 1.4	14.70 ± 0.22	1.19	30
TU29	gneiss	Uludağ Group	500	20	0.38	34	0.64	563	99.99	0.95	4534	10.5 ± 1.9	-	-	-
TU31	metagranite	S. Uludağ metagranite	1440	20	0.41	28	0.77	528	97.73	0.95	4520	9.2 ± 1.8	14.10 ± 0.23	1.24	30
TU105	gneiss	Uludağ Group	1356	20	0.56	41	0.55	378	99.89	1.11	5272	22.0 ± 3.6	-	-	-
TU103	gneiss	clast in the Neogene	~830	20	0.35	45	0.49	628	97.18	1.09	5156	14.3 ± 2.2	-	-	-
TU32	granodiorite	Topuk pluton	950	20	1.59	84	0.89	472	40.92	0.95	4490	30.4 ± 4.1	13.99 ± 0.29	1.44	25
TU24	acidic tuff	Neogene	570	20	2.45	158	1.63	1050	49.17	0.96	4550	26.3 ± 2.3	15.09 ± 0.10	1.00	97
TU102	sandstone	Lower Jurassic	~850	8	8.43	129	0.92	138	65.98	1.09	5175	184.1 ± 22.8	-	-	-
TU109	sandstone	Upper Triassic	~440	19	5.66	336	2.63	1562	0.00	1.12	5291	39.4 ± 4.8	-	-	-

Note: Central ages calculated using dosimeter glass CN5 and ζ-CN5 = 369.01 ± 3.3. ρ_s, spontaneous track densities (× 105 cm^{-2}) measured in internal mineral surfaces; N_s, total number of spontaneous tracks; ρ_i and ρ_d, induced and dosimeter track densities (× 106 cm^{-2}) on external mica detectors (g = 0.5); N_i and N_d, total numbers of tracks; $P(\chi^2)$, probability of obtaining χ^2 value for ν degrees of freedom (where ν = number of crystals - 1); a probability >5% is indicative of a homogeneous population.

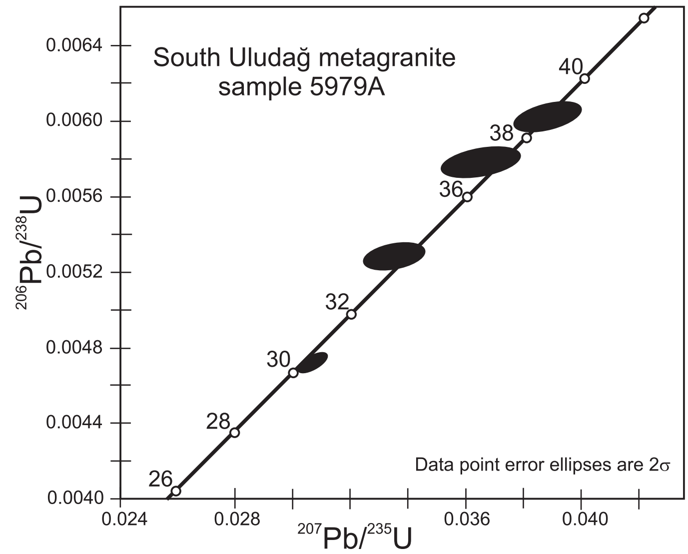

Figure 12. U-Pb concordia diagram for the South Uludağ metagranite.

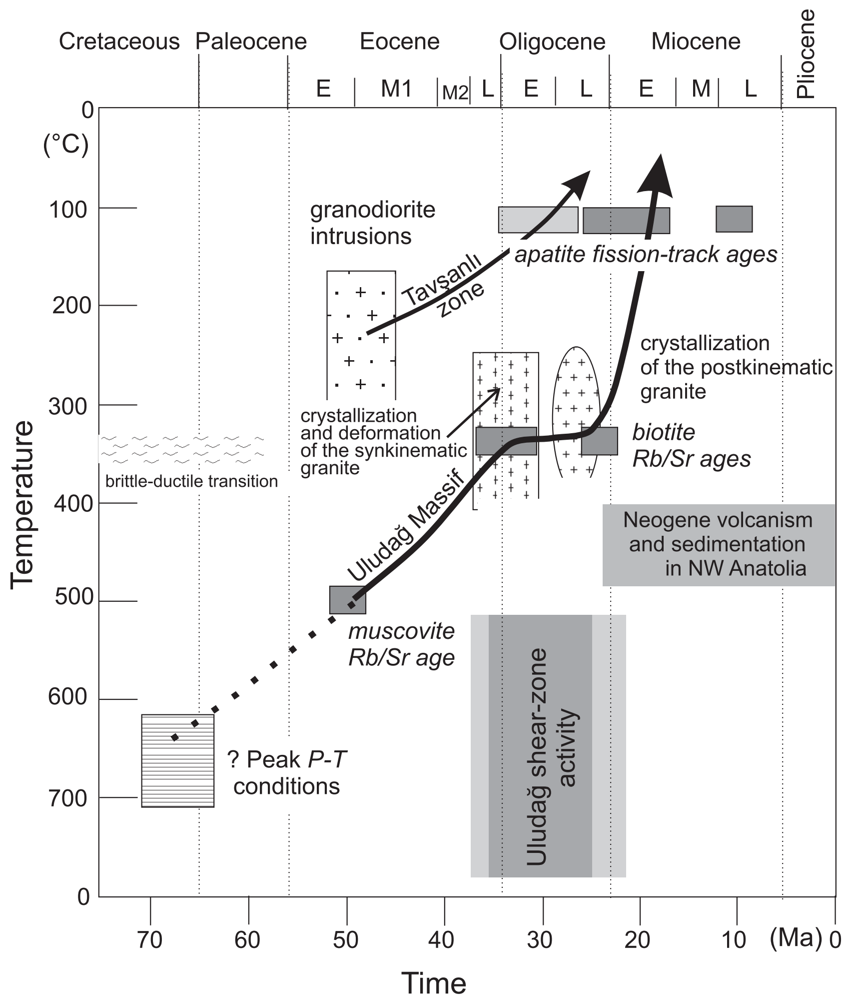

Figure 13. Temperature-time-depth diagram illustrating the thermochronological evolution of the Uludağ Massif and the Tavşanlı zone. P-T—pressure-temperature.

Rb/Sr muscovite age, using a cooling rate of 12 °C/m.y., would give a latest Cretaceous to early Paleocene age (ca. 64 Ma) estimate for the peak temperatures conditions of 670 °C. This age is compatible with the regional tectonics, since the continental collision between the Anatolide-Taurides and the Pontides occurred during the latest Cretaceous–early Paleocene (Okay and Tüysüz, 1999).

Apatite Fission-Track Data

Apatite fission-track (AFT) ages indicate the time the rocks cooled down to ~120 °C. At these relatively low temperatures, the metamorphic rocks of the Uludağ Group and the Uludağ granites can be considered as a single unit. Our AFT ages from the Uludağ Massif are Oligocene and Miocene, ranging from 28.9 ± 3.7 Ma to 9.2 ± 1.8 Ma (Table 5). Although the samples were collected from a vertical section of more than 1600 m, the AFT ages do not show a clear correlation with elevation, and they exhibit abrupt variations. Despite these complexities, two broad AFT age groups can be recognized: (1) late Oligocene–early Miocene AFT ages with a cluster at 22–20 Ma, and (2) late Miocene AFT ages (10–9 Ma), which are restricted to the margins of the range. The older ages represent continuation of the moderately fast exhumation documented by the Rb/Sr mica ages (Fig. 13). Long track lengths (>14.5 μm) with low standard deviations (<1.3 μm) in the apatites indicate rapid cooling through the partial annealing zone from ~120 °C to ~60 °C. The younger ages may indicate a second phase of accelerated uplift in the late Miocene.

The Uludağ Massif as a Strike-Slip Shear Zone—Timing and Displacement

We propose that the Uludağ Group is an exhumed midcrustal portion of a right-lateral strike-slip shear zone. This is based on the following criteria: (1) its location at the tip of the Eskişehir fault zone, (2) the ubiquitous subhorizontal mineral lineations, (3) the presence of the synkinematic South Uludağ metagranite, (4) foliation with a consistent NNW strike, and (5) the subparallel alignment of the lineation (~114°), the strike of foliation (~114°), the long axis of the South Uludağ metagranite (110°), the Eskişehir fault zone (109°), and the mountain range (~117°). The spatial association between the Uludağ shear zone and the Eskişehir fault zone, and the Bouguer gravity anomaly changes along this lineament suggest that the Uludağ shear zone extends at depth southeastward underneath the Eskişehir fault. The Uludağ shear zone and the Eskişehir fault represent the same structure exposed at different crustal levels. This is also suggested by the observation that the Mesozoic to Eocene strata have been stripped off in an ~20-km-wide belt north of the Eskişehir fault (Konak, 2002; Turhan, 2002). We use the term Uludağ shear zone to describe a midcrustal right-lateral Oligocene shear zone that is inferred to exist underneath the Eskişehir fault. Although a spatial equivalence between these two structures is obvious, a temporal link cannot be demonstrated. The Uludağ shear zone was formed under strike slip; the present movement along the Eskişehir fault is, however, predominantly downdip.

The inception of the Uludağ shear zone is poorly constrained. The 48 Ma Topuk pluton and the Nalınlar intrusion are aligned with the Göktepe and Soğukpınar faults (Fig. 6), suggesting structural control during their intrusion. However, these plutons are not deformed, and there is no information on the nature of the shear-zone activity during the early and middle Eocene. The synkinematic South Uludağ metagranite, which was emplaced into and deformed by a right-lateral strike-slip shear zone, indicates that the shear zone was active in the latest Eocene and Oligocene between ca. 38 Ma and ca. 27 Ma. The 27 Ma Central Uludağ granite cuts the ductile fabrics in the Uludağ gneisses, indicating that the Uludağ shear zone had ceased its activity by that time. Another upper limit to the shear-zone activity is provided by the Upper Miocene İnegöl Basin, which lies along strike of the Uludağ shear zone.

The 9-km-thick Uludağ shear zone, with its intense foliation and subhorizontal lineation, suggests a major amount of cumulative displacement. Unfortunately, the pre-Eocene geology on both sides of the Eskişehir fault is different, which precludes estimation of the total offset on the basis of geological tie lines. Nevertheless, the total offset along the Uludağ shear zone can be estimated using the Bouguer gravity isomilligals, which are consistently offset in a right-lateral sense (Fig. 4). The offsets of the −25 and −50 mgal isomilligals are ~80 and ~140 km, respectively. The 400-km-long Eocene plutonic belt in northwest Turkey is also offset by ~100 km along the Uludağ shear zone (cf. Figure 3 in Okay and Satır, 2006). The İzmir-Ankara suture is offset by ~170 km along the Uludağ shear zone, although this is less reliable because the original early Paleocene structure could have followed a similar trend.

The interpretation of the structural, isotopic, and geophysical data suggest that the Uludağ shear zone was active in the latest Eocene and Oligocene (ca. 38 Ma to ca. 27 Ma) and accommodated a total right-lateral slip of 100 ± 20 km. The estimated offset has the right order of magnitude expected from a displacement-to-length relationship in faults (Cowie and Scholz, 1992).

EXHUMATION OF THE ULUDAĞ SHEAR ZONE

Here, we review the available stratigraphic, structural, and thermochronological evidence for the exhumation of the Uludağ shear zone, starting with the exhumation history of the Tavşanlı zone south of the İzmir-Ankara suture and that of the hanging wall of the Uludağ Massif

The Tavşanlı Zone—South of the İzmir-Ankara Suture

The exhumation of the Eocene intrusions south of the İzmir-Ankara suture can be used as a proxy for that of the Tavşanlı zone. The Ar-Ar hornblende and AFT ages from the Topuk pluton are 47.8 ± 0.4 Ma (Harris et al., 1994) and 30.4 ± 4.1 Ma (Table 5), respectively. The depth of emplacement of the neighboring co-genetic and coeval Tepelce and Orhaneli intrusions, determined from their contact metamorphic assemblages and from the mineral chemistry of the granodiorites, is 7 ± 3 km (Harris et al., 1994; Okay and Satır, 2006). A similar depth of emplacement for the Topuk granodiorite would give total exhumation of 3–4 km and an average exhumation rate of 0.2–0.3 km/m.y. in the middle Eocene–early Oligocene interval (48 Ma to 30 Ma) for the Tavşanlı zone (Fig. 13). The Eocene granodiorites were on the surface by the early Miocene; biotites from the acidic tuffs, which lie unconformably over the Orhaneli pluton, have yielded a 17.6 ± 0.2 Ma (early Miocene) Ar-Ar age (Okay et al., 1998).

The Hanging Wall of the Uludağ Massif

The preservation of the Jurassic regional unconformity in the hanging wall west of the Uludağ Massif (Figs. 6 and 7A) indicates minimal amounts of bedrock erosion in this region. This is confirmed by the AFT age from a sample of Lower Jurassic sandstone, which yielded an Early Jurassic age (184.1 ± 22.8 Ma; Table 5), showing that the Jurassic sequence was never buried more than a few kilometers. Conversely, the northeastern hanging wall of the Uludağ Massif was more deeply buried and then exhumed, as indicated by a middle Eocene AFT age of 39.4 ± 4.8 Ma from the Triassic arkosic sandstones of the Karakaya Complex (Table 5). However, the presence of unmetamorphosed Permian limestone blocks, Triassic sandstones, and Cretaceous limestones in this part of the hanging wall (Ketin, 1947; Imbach, 1992) shows that the Triassic rocks were buried not deeper than 4–5 km during the Mesozoic and Tertiary. Furthermore, the AFT age shows that the exhumation occurred during the middle Eocene and is unrelated to the Oligocene strike-slip activity.

Neogene Basins

Neogene basins along Tertiary shear zones can provide insights into the timing of strike-slip activity and the mechanism of exhumation (e.g., Schoenbohm et al., 2005). Several Neogene basins with terrigenous sediments occur along the Uludağ shear zone (Fig. 6).

The Deliler and Erenler Basins

These elongate and narrow basins, which have sedimentary fills <500 m thick, lie along the Soğukpınar and Göktepe faults (Fig. 6). The basin fill consists mainly of terrigenous conglomerates, pebbly sandstones, sandstones, and rare mud rocks. The dominant lithology is thick bedded to massive conglomerates; the poorly sorted clasts, up to 4 m across, are mainly peridotite, dolerite, and granodiorite with minor gneiss. Caliche horizons are common in the sandstones, and the succession includes several paleosols. In the stratigraphically upper parts of the Erenler Basin, there are also several-meter-thick acidic tuff beds. One of them yielded an AFT age of 26.3 ± 2.3 Ma (Table 5), indicating a late Oligocene age for the Erenler Basin and, by analogy, for the Deliler Basin. The Oligocene AFT age (30.4 ± 4.1 Ma) from the Topuk granodiorite, which forms part of the basement, provides a lower age limit for the basinal sediments. The Deliler and Erenler Basins are older than the other Neogene sequences in western Turkey, which have late early Miocene to Pliocene mammals, pollen, and ostracoda (e.g., Bernor and Tobien, 1990; Emre et al., 1998; Kaya et al., 2007) and early to middle Miocene isotopic ages (23–15 Ma; e.g., Seyitoğlu and Scott, 1992; Aldanmaz et al., 2000; Erkül et al., 2005; Purvis et al., 2005).

Poor sorting, dominance of the unstable peridotite clasts in the conglomerates, and the lensoid sandstone lenses in the sequence indicate deposition by streams and little long-distance transport. The stratigraphic similarity between the Erenler and Deliler Basins suggests the presence of a late Oligocene integrated fluvial drainage along the Uludağ fault zone (Fig. 14B). The Erenler and Deliler Basins are little deformed. No folds or thrusts are observed. The locally steep bedding is related to tilting by faulting. The Göktepe fault can be seen to cut and shear the conglomerates of the Erenler Basin in a steeply north-dipping fault zone that is several meters wide.

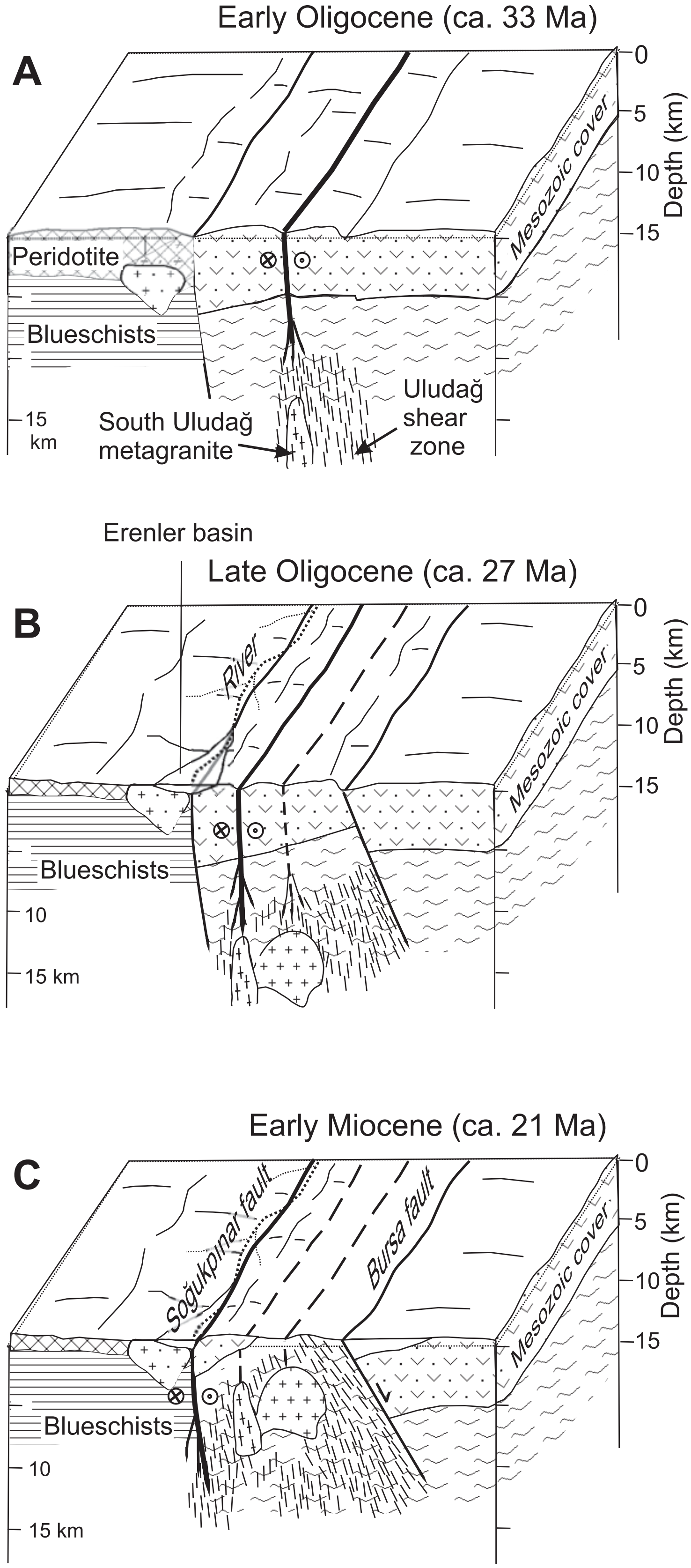

Figure 14. Block diagrams showing the exhumation of the Uludağ shear zone in the Oligocene-Miocene.

The İnegöl Basin

The İnegöl Basin extends in a WNW-ESE direction along the trend of the Uludağ shear zone (Fig. 2). The alluvial sediments in the center of the present-day basin, bounded by active normal faults (Şaroğlu et al., 1992), indicate that the basin is still active and subsiding. The İnegöl Basin is filled by lacustrine and fluviatile deposits, about one kilometer thick, which lie unconformably over a heterogeneous basement that consists of the Lower Karakaya Complex, Cretaceous metamorphic and ophiolitic rocks, and Eocene granodiorite (Fig. 6). The contact with the Uludağ Group is covered by scree and landslides; however, ubiquitous gneiss boulders in the basal conglomerates suggest that the Neogene sediments may lie unconformably over the Uludağ shear zone.

The Neogene sequence in the İnegöl Basin starts with very poorly sorted, thickly bedded to massive conglomerates, several hundred meters thick, intercalated with thick sandstone beds. The clasts, up to 4 m across, include gneiss, mica schist, granodiorite, dacite, and marble, derived from the Uludağ Massif and the Eocene granodiorites. We dated a gneiss clast from the conglomerates using the AFT technique (Table 5). A middle Miocene AFT age of 14.3 ± 2.2 Ma provides a lower age limit for the İnegöl Basin and indicates that the Uludağ Massif was being eroded during the inception of the basin.

The conglomerates of the İnegöl Basin pass up into a lacustrine turbiditic sequence of medium- to thin-bedded sandstone, siltstone, and shale that is over 600 m thick (Kaymakçı, 1991). Thin, laterally discontinuous coal seams occur in the transition zone between the conglomerates and the lacustrine turbidites. Current bedding and slumps in the turbiditic sandstones indicate a westerly to southwesterly sediment source. Based on vertebrate fossils, mainly *Hipparion* sp., a late Miocene age is assigned to the sediments of the İnegöl Basin (Genç, 1986), which is compatible with the AFT age from the gneiss clast.

The sedimentary basin fill of the İnegöl Basin is deformed into a broad and complex syncline with an axis subparallel to the Eskişehir fault. The syncline was formed through basement uplift in the south and back-tilting along a normal fault in the north. There are also local folds with short (meters to tens of meters) wavelengths in the thinly bedded lacustrine turbidites.

Uludağ Massif

As documented already, the hanging wall of the Uludağ shear zone has been stable with respect to Earth's surface since the Eocene, and the Tavşanlı zone has been largely at the present erosion level since the late Oligocene. In contrast, the Uludağ Massif has been exhumed by ~10 km since the early Oligocene and by at least ~3.5 km since the early Miocene, as estimated from the ca. 33 Ma Rb/Sr biotite and ca. 21 Ma AFT ages from the gneisses using a 30 °C/m.y. average geotherm.

There is little evidence for exhumation of the Uludağ Massif during the Oligocene shear-zone activity. Mineral stretching lineations are subhorizontal, indicating no vertical motion during ductile shear. No major structures indicative of transpression or transtension are recognized in the late Oligocene basins south of Uludağ. The clasts in the conglomerates in these basins are predominantly composed of ultramafic and mafic rocks. The absence of ductile exhumation structures suggests that the Uludağ shear zone cooled isobarically below the ductile-brittle transition after the cessation of shear-zone activity and was then exhumed along the Bursa, Soğukpınar, and Kirazlı faults during the early Miocene (Fig. 13). The cluster of AFT ages around 22–20 Ma with long track lengths in apatite grains indicates fast cooling, accelerated uplift, and increased denudation in the early Miocene. The uniform metamorphic grade of the Uludağ shear zone also shows that exhumation occurred along the boundary faults. Several of the Neogene basins in northwest Anatolia date back to the early Miocene. The late Oligocene–early Miocene (25–21 Ma) was a period of major NNE-directed extension in ductile middle crust in western Anatolia, as documented in the Kazdağ and Simav core complexes (Figs. 1 and 2; Okay and Satır, 2000; Işık and Tekeli, 2001; Işık et al., 2004; Thomson and Ring, 2006). Exhumation was aided by the density and viscosity inversion between the warm quartzo-feldspathic Uludağ Massif and the overlying cold mafic Lower Karakaya Complex. The Uludağ ductile shear zone was unroofed by the middle to late Miocene as shown by (1) the 14.3 ± 2.2 Ma AFT age from the gneiss clast in the İnegöl Basin, and (2) the late Miocene age of the basin itself, which lies along the eastward continuation of the shear zone (Fig. 6).

Thermochronological, stratigraphic, and structural arguments indicate that major exhumation of the Uludağ shear zones occurred during the early Miocene. The exhumation occurred through extrusion along a fault-bounded crustal channel, possibly aided by density and viscosity inversion.

CONCLUSIONS

The Uludağ Massif represents an exhumed segment of a ductile right-lateral shear zone that was active during the latest Eocene and Oligocene (38–27 Ma) and that accommodated 100 ± 20 km of total slip. The amphibolite-facies regional metamorphism of the Uludağ Group predates the shear-zone activity, as shown by the Eocene Rb/Sr muscovite ages. Regional metamorphism occurred during the latest Cretaceous and early Paleocene, which was characterized by a period of crustal thickening along the suture following the continental collision between the Pontides and the Anatolide-Taurides. The metamorphism would have created a ductile middle crust, which would have facilitated the localization of the strike-slip activity along the suture, similar to the case of the Insubric line in the Western Alps (e.g., Schmid et al., 1989).

The Uludağ shear zone forms part of a set of pre–late Miocene strike-slip faults in northwest Turkey, including the Terzili fault in Thrace (Fig. 2; Perinçek, 1991) and the latest Eocene–Oligocene Kapıdağı shear zone (Aksoy, 1998). Recently, the Ganos segment of the North Anatolian fault in Thrace was shown to be active during the Oligocene (Zattin et al., 2005), and other segments may have been active even earlier (Uysal et al., 2006). Jolivet (2001) showed that the Oligocene-Miocene finite strain field is similar, in terms of direction and rates of extension, to the active strain pattern in the Aegean, as recorded by GPS data. The presence of major right-lateral strike-slip faults in Anatolia completes the picture and shows that during the Oligocene-Miocene, the tectonics in the Aegean-Anatolian region resembled that of the present day.

Westward translation of the Anatolian microplate into the north-south–extending Aegean region dominates the present tectonics of the Eastern Mediterranean (Fig. 1; McKenzie, 1972; Reilinger et al., 2006). Extension in the Aegean Sea and the surrounding region is caused by slab suction along the Aegean subduction zone. It dates back to the Oligocene, as shown by the age of the metamorphic core complexes in the Aegean islands and western Anatolia (e.g., Jolivet and Faccenna, 2000; Okay and Satır, 2000). The inception of the westward translation of the Anatolian plate was, on the other hand, related to the Miocene collision between Arabia and Eurasia (e.g., Şengör et al., 1985). However, the presence of major right-lateral strike-slip faults during the Oligocene indicates that slab suction from the Hellenic trench was and is the main mechanism for the westward translation of Anatolia.

Exhumation of the Uludağ shear zone occurred during the early Miocene. The high-grade gneisses of the Uludağ shear zone were exhumed for ~10 km vertical distance in a fault-bounded crustal-scale channel with little subsidence or uplift in the adjacent blocks (Fig. 14).

Oligocene-Miocene metamorphic core complexes are common in the Aegean and in western

Turkey. They were formed and exhumed under extension, as shown by their synmetamorphic downdip stretching lineations and low-pressure–high-temperature metamorphism coeval with extension. The Uludağ Massif differs from the other Aegean core complexes because it was shaped under right-lateral strike slip and not under extension.

The Uludağ shear zone has a deformation history going back to 50 Ma, and it is still active as the oblique-slip Eskişehir fault; however, the main strike-slip activity occurred for 10 m.y. in the latest Eocene–Oligocene (38–27 Ma), when it accommodated 100 ± 20 km of right-lateral strike-slip motion. The collision of the Arabian and Anatolian plates in the Miocene might have created a new stress regime that resulted in a switch of the main strike-slip activity from the Uludağ shear zone to the North Anatolian fault. The case of the Uludağ shear zone illustrates that, although strain is localized over geological time scales, strike-slip fault activity can switch between faults on time scales of ~10 m.y.

ACKNOWLEDGMENTS

We thank the İstanbul Technical University Research Fund (project no. 31573), the Turkish Academy of Sciences, and MIUR (Italian Department of Public Education, University and Research) for partial support. Field work in the region in the years 2000 to 2004 was supported by TÜBİTAK projects. Vincenzo Picotti is thanked for help during field work in 2005. Thanks are also due to Rainer Altherr for the friendly access to the microprobe facility. We thank Giulio Viola, Chris Morley, and Stefano Mazzoli for constructive and detailed reviews.

REFERENCES CITED

Aksoy, R., 1998, Strain analysis of the Kapıdağı Peninsula shear zone in the Ocaklar granitoid, NW Turkey: Turkish Journal of Earth Sciences, v. 7, p. 79–85.

Aldanmaz, E., Pearce, J.A., Thirlwall, M.F., and Mitchel, J.G., 2000, Petrogenetic evolution of late Cenozoic, post-collision volcanism in western Anatolia, Turkey: Journal of Volcanology and Geothermal Research, v. 102, p. 67–95, doi: 10.1016/S0377-0273(00)00182-7.

Altunel, E., and Barka, A., 1998, Neotectonic activity of the Eskişehir fault zone between İnönü and Sultandere: Türkiye Jeoloji Bülteni, v. 2, p. 41–52.

Anczkiewicz, R., Viola, G., Müntener, O., Thirlwall, M.F., Villa, I.M., and Quong, N.Q., 2007, Structure and shearing conditions in the Day Nui Con Voi massif: Implications for the evolution of the Red River shear zone in northern Vietnam: Tectonics, v. 26, p. TC2002, doi: 10.1029/2006TC001972

Ateş, A., Kearey, P., and Tufan, S., 1999, New gravity and magnetic anomaly maps of Turkey: Geophysical Journal International, v. 136, p. 499–502, doi: 10.1046/j.1365-246X.1999.00732.x.

Barka, A.A., 1992, The North Anatolian fault zone: Annalae Tectonicae, v. 6, p. 164–195.

Barka, A., Reilinger, R., Şaroğlu, F., and Şengör, A.M.C., 1995, The Isparta angle: Its importance in the neotectonics of the Eastern Mediterranean region, *in* PiŞkin, Ö., et al., eds., Proceedings of the International Earth Science Colloquium on the Aegean Region: Ismir, University of 9 Eylul, p. 3–17.

Bernor, R.L., and Tobien, H., 1990, The mammalian geochronology and biogeography of PaŞalar (middle Miocene, Turkey): Journal of Human Evolution, v. 19, p. 551–568, doi: 10.1016/0047-2484(90)90064-I.

Bingöl, E., Delaloye, M., and Ataman, G., 1982, Granitic intrusions in western Anatolia: A contribution to the geodynamic study of this area: Eclogae Geologicae Helvetiae, v. 75, p. 437–446.

Bohlen, S.R., and Liotta, J.J., 1986, A barometer for garnet amphibolites and garnet granulites: Journal of Petrology, v. 27, p. 1025–1034.

Bohlen, S.R., Wall, V.J., and Boettcher, A.L., 1983, Experimental investigations and geological applications of equilibria in the system FeO-TiO_2-Al_2O_3-SiO_2-H_2O: The American Mineralogist, v. 68, p. 1049–1058.

Bozkurt, E., 2001, Neotectonics of Turkey—A synthesis: Geodinamica Acta, v. 14, p. 3–30, doi: 10.1016/S0985-3111(01)01066-X.

Çemen, İ., Göncüoğlu, M.C., and Dirik, K., 1999, Structural evolution of the Tuzgölü Basin in Central Anatolia, Turkey: The Journal of Geology, v. 107, p. 693–706, doi: 10.1086/314379.

Cliff, R.A., 1985, Isotopic dating in metamorphic belts: Journal of the Geological Society [London], v. 142, p. 97–110, doi: 10.1144/gsjgs.142.1.0097.

Cowie, P.A., and Scholz, C.H., 1992, Displacement-length scaling relationship for faults: Data synthesis and discussion: Journal of Structural Geology, v. 14, p. 1149–1156, doi: 10.1016/0191-8141(92)90066-6.

Delaloye, M., and Bingöl, E., 2000, Granitoids from western and northwestern Anatolia: Geochemistry and modeling of geodynamic evolution: International Geology Review, v. 42, p. 241–268.

Dewey, J.F., Hempton, M.R., Kidd, W.S.F., Şaroğlu, F., and Şengör, A.M.C., 1986, Shortening of continental lithosphere: The neotectonics of Eastern Anatolia—A young collision zone, *in* Coward, M.P. and Ries, A.C., eds., Collision tectonics: Geological Society of London Special Publication 19, p. 3–36.

Emre, Ö., Erkal, T., Tchepalyga, A., Kazancı, N., Keçer, M., and Ünay, E., 1998, Neogene-Quaternary evolution of the eastern Marmara region, northwest Turkey: Bulletin of the Mineral Research and Exploration Institute of Turkey, v. 120, p. 119–145.

Erkül, F., Helvacı, C., and Sözbilir, H., 2005, Stratigraphy and geochronology of the early Miocene volcanic units in the Bigadiç borate basin, Western Turkey: Turkish Journal of Earth Sciences, v. 14, p. 227–253.

Ferry, J.M., and Spear, F.S., 1978, Experimental calibration of partitioning of Fe and Mg between biotite and garnet: Contributions to Mineralogy and Petrology, v. 66, p. 113–117, doi: 10.1007/BF00372150.

Gapais, D., and Le Corre, C., 1980, Is the Hercynian belt of Brittany a major shear zone: Nature, v. 288, p. 574–575, doi: 10.1038/288574a0.

Genç, Ş., 1986, Geology of the region between Uludağ and the Lake of İznik: Maden Tetkik ve Arama Genel Müdürlüğü Open-File Report 7852, 122 p. (in Turkish).

Gradstein, F.M., Ogg, J.G., Smith, A.G., Bleeker, W., and Lourens, L.J., 2004, A new geological time scale with special reference to Precambrian and Neogene: Episodes, v. 27, p. 83–100.

Graham, C.M., and Powell, R., 1984, A garnet-hornblende geothermometer: Calibration, testing and application to the Pelona Schist, southern California: Journal of Metamorphic Geology, v. 2, p. 13–31, doi: 10.1111/j.1525-1314.1984.tb00282.x.

Harris, N.B.W., Kelley, S., and Okay, A.I., 1994, Post-collision magmatism and tectonics in northwest Anatolia: Contributions to Mineralogy and Petrology, v. 117, p. 241–252, doi: 10.1007/BF00310866.

Hoisch, T.D., 1990, Empirical calibration of six geobarometers for the mineral assemblage quartz + muscovite + biotite + plagioclase + garnet: Contributions to Mineralogy and Petrology, v. 104, p. 225–234, doi: 10.1007/BF00306445.

Hoisch, T.D., 1991, Equilibria within the mineral assemblage quartz + muscovite + biotite + garnet + plagioclase, and implications for the mixing properties of octahedrally-coordinated cations in muscovite and biotite: Contributions to Mineralogy and Petrology, v. 108, p. 43–54, doi: 10.1007/BF00307325.

Holland, T., and Blundy, J., 1994, Non-ideal interactions in calcic amphiboles and their bearing on amphibole-plagioclase thermometry: Contributions to Mineralogy and Petrology, v. 116, p. 433–447, doi: 10.1007/BF00310910.

Holland, T.J.B., and Powell, R., 1998, An internally consistent thermodynamic data set for phases of petrological interest: Journal of Metamorphic Geology, v. 16, p. 309–343, doi: 10.1111/j.1525-1314.1998.00140.x.

Hubert-Ferrari, A., Armijo, R., King, G.C.P., Meyer, B., and Barka, A., 2002, Morphology, displacement, and slip rates along the North Anatolian fault, Turkey: Journal of Geophysical Research–Solid Earth, v. 107, no. B10, 2235, doi: 10.1029/2001JB000393.

Imbach, T., 1992, Thermalwasser von Bursa. Geologische und Hydrogeologische Untersuchungen am Berg Uludağ (NW-Türkei) [Ph.D. thesis]: Zürich, Swiss Federal Institute of Technology, 178 p.

Işık, V., and Tekeli, O., 2001, Late orogenic crustal extension in the northern Menderes Massif (western Turkey): Evidence for metamorphic core complex formation: International Journal of Earth Sciences, v. 89, p. 757–765, doi: 10.1007/s005310000105.

Işık, V., Tekeli, O., and Seyitoğlu, G., 2004, The $^{40}Ar/^{39}Ar$ age of extensional ductile deformation and granitoid intrusion in the northern Menderes core complex: Implications for the initiation of extensional tectonics in western Turkey: Journal of Asian Earth Sciences, v. 23, p. 555–566, doi: 10.1016/j.jseaes.2003.09.001.

Jäger, E., Niggli, E., and Wenk, E., 1967, Rb-Sr Altersbestimmungen an Glimmern der Zentralalpen: Beiträge zu der Geologische Karte der Schweiz NF134, 67 p.

Jégouzo, P., 1980, The South Armorican shear zone: Journal of Structural Geology, v. 2, p. 39–47, doi: 10.1016/0191-8141(80)90032-2.

Jolivet, L., 2001, A comparison of geodetic and finite strain in the Aegean, geodynamic implications: Earth and Planetary Science Letters, v. 187, p. 95–104, doi: 10.1016/S0012-821X(01)00277-1.

Jolivet, L., and Faccenna, C., 2000, Mediterranean extension and the Africa-Eurasia collision: Tectonics, v. 19, p. 1095–1106, doi: 10.1029/2000TC900018.

Jolivet, L., Famin, V., Mehl, C., Parra, T., Aubourg, C., Hébert, R., and Phillippot, P., 2004, Strain localization during crustal-scale boudinage to form extensional metamorphic domes in the Aegean Sea., *in* Whitney, D.L., et al., eds., Gneiss domes in orogeny: Geological Society of America Special Paper 380, p. 185–210.

Karacık, Z., and Yılmaz, Y., 1998, Geology of the ignimbrites and the associated volcano-plutonic complex of the Ezine area, northwest Anatolia: Journal of Volcanology and Geothermal Research, v. 85, p. 251–264, doi: 10.1016/S0377-0273(98)00058-4.

Kaya, O., Ünay, E., GöktaŞ, F., and Saraç, G., 2007, Early Miocene stratigraphy of central West Anatolia, Turkey: Implications for the tectonic evolution of the Eastern Aegean area: Geological Journal, v. 42, p. 85–109, doi: 10.1002/gj.1071.

Kaymakçı, N., 1991, Neotectonic Characteristics of the İnegöl Basin (Bursa, Turkey) [M.S. thesis]: Ankara, Turkey, Middle East Technical University, 73 p.

Ketin, İ., 1947, Über die Tektonik des Uludağ–Massivs: Türkiye Jeoloji Kurumu Bülteni, v. 1, p. 60–88.

Ketin, İ., 1984, New developments in the thrust-nappe tectonics of Turkey with the example of the Uludağ Massif, *in* Proceedings of the Ketin Symposium: Ankara, Geological Society of Turkey, p. 19–36 (in Turkish).

Koçyiğit, A., 2005, The Denizli graben-horst system and the eastern limit of western Anatolian continental extension: Basin fill, structure, deformational mode, throw amount and episodic evolutionary history: SW Turkey: Geodinamica Acta, v. 18, p. 167–208, doi: 10.3166/ga.18.167-208.

Kohn, M.J., and Spear, F.S., 1990, Two new geobarometers for garnet amphibolites, with applications to southeastern Vermont: The American Mineralogist, v. 75, p. 89–96.

Konak, N. 2002, Geological map of Turkey, İzmir sheet: Ankara, Maden Tetkik ve Arama Genel Müdürlüğü, scale 1:500,000, 1 sheet.

Koziol, A.M., and Newton, R.C., 1988, Redetermination of the anorthite breakdown reaction and improvement of the plagioclase-garnet-Al_2SiO_5-quartz geobarometer: The American Mineralogist, v. 73, p. 216–223.

Leloup, P.H., Harrison, T.M., Ryerson, F. J., Chen, W.J., Li, Q., Tapponier, P., and Lacassin, R., 1993, Structural, petrological and thermal evolution of a Tertiary ductile strike-slip shear zone, Diancang Shan, Yunnan: Journal of Geophysical Research–Solid Earth, v. 98, p. 6715–6743.

Leloup, P.H., Ricard, Y., Battaglia, J., and Lacassin, R., 1999, Shear heating in continental strike-slip shear zones: Numerical modelling and case studies: Geophysical Journal International, v. 136, p. 19–40, doi: 10.1046/j.1365-246X.1999.00683.x.

Lisenbee, A., 1971, The Orhaneli ultramafic-gabbro thrust sheet and its surroundings, *in* Campbell, A.S., ed., Geology and history of Turkey: Tripoli, Libya, Petroleum Exploration Society, p. 349–360.

McKenzie, D.P., 1972, Active tectonics of the Mediterranean region: Geophysical Journal of the Royal Astronomical Society, v. 30, p. 109–185.

Ocakoğlu, F., 2007, A re-evaluation of the Eskisehir fault zone as a recent extensional structure in NW Turkey: Journal of Asian Earth Sciences, v. 31, p. 91–103.

Okay, A.I., and Satır, M., 2000, Coeval plutonism and metamorphism in a latest Oligocene metamorphic core complex in northwest Turkey: Geological Magazine, v. 137, p. 495–516, doi: 10.1017/S0016756800004532.

Okay, A.I., and Satır, M., 2006, Geochronology of Eocene plutonism and metamorphism in northwest Turkey: Evidence for a possible magmatic arc: Geodinamica Acta, v. 19, p. 251–266, doi: 10.3166/ga.19.251-266.

Okay, A.I., and Tüysüz, O., 1999, Tethyan sutures of northern Turkey, *in* Durand, B., et al., eds., The Mediterranean basins: Tertiary extension within the Alpine orogen: Geological Society of London Special Publication 156, p. 475–515.

Okay, A.I., Harris, N.B.W., and Kelley, S.P., 1998, Exhumation of blueschists along a Tethyan suture in northwest Turkey: Tectonophysics, v. 285, p. 275–299, doi: 10.1016/S0040-1951(97)00275-8.

Özsayın, E., and Dirik, K., 2007, Quaternary activity of the Cihanbeyli and Yeniceoba fault zones: İnönü-Eskişehir fault system, Central Anatolia: Turkish Journal of Earth Sciences, v. 16, p. 471–492.

Öztunalı, Ö., 1973, Geochronology and Petrology of the Uludağ (Northwest Anatolia) and Eğrigöz (West Anatolia) Massifs: İstanbul Üniversitesi Fen Fakültesi Monografileri (Tabii İlimler Kısmı) 23, 115 p. (in Turkish).

Passchier, C.W., and Trouw, R.A.J., 1998, Micro-Tectonics: Berlin, Springer Verlag, 289 p.

Perinçek, D., 1991, Possible strand of the North Anatolian Fault in the Thrace Basin, Turkey—An interpretation: American Association of Petroleum Geologists Bulletin, v. 57, p. 241–257.

Powell, R., and Holland, T.J.B., 1988, An internally consistent thermodynamic dataset with uncertainties and correlations: 3. Application methods, worked examples and a computer program: Journal of Metamorphic Geology, v. 6, p. 173–204, doi: 10.1111/j.1525-1314.1988.tb00415.x.

Purvis, M., Robertson, A., and Pringle, M., 2005, Ar^{40}-Ar^{39} dating of biotite and sanidine in tuffaceous sediments and related intrusive rocks: Implications for the early Miocene evolution of the Gördes and Selendi Basins, W Turkey: Geodinamica Acta, v. 18, p. 239–253, doi: 10.3166/ga.18.239-253.

Reilinger, R., et al., 2006, GPS constraints on continental deformation in the Africa-Arabia-Eurasia continental collision zone and implications for the dynamics of plate interactions: Journal of Geophysical Research, v. 111, B05411, doi: 10.1029/2005JB004051.

Robertson, A.H.F., and Grasso, M., 1995, Overview of the Late Tertiary–Recent tectonic and palaeo-environmental development of the Mediterranean region: Terra Nova, v. 7, p. 114–127, doi: 10.1111/j.1365-3121.1995.tb00680.x.

Sandison, D., 1855, Notice of the earthquakes of Brussa: Quarterly Journal of the Geological Society of London, v. 11, p. 543–544.

Şaroğlu, F., Emre, Ö., and KuŞçu, İ., 1992. Active fault map of Turkey: Ankara, Turkey, General Directorate of the Mineral Research and Exploration, 2 sheets, scale 1:2,000,000.

Schärer, U., Zhang, L.S., and Tapponnier, P., 1994, Duration of strike-slip movements in large shear zones: The Red River belt, China: Earth and Planetary Science Letters, v. 126, p. 379–397, doi: 10.1016/0012-821X(94)90119-8.

Schmid, S.M., Aebli, H.R., Heller, F., and Zingg, A., 1989, The role of the Periadriatic Line in the tectonic evolution of the Alps, *in* Coward, M.P., et al., eds., Alpine tectonics: Geological Society of London Special Publication 45, p. 153–171.

Schoenbohm, L.M., Burchfiel, B.C., Liangzhong, C., and Jiyun, Y., 2005, Exhumation of the Ailao Shan shear zone recorded by Cenozoic sedimentary rocks, Yunnan Province, China: Tectonics, v. 24, TC6015, doi: 10.1029/2005TC001803.

Şengör, A.M.C., Görür, N., and Şaroğlu, F., 1985, Strike-slip faulting and related basin formation in zones of tectonic escape: Turkey as a case study, *in* Biddle, K.D., and Christie-Blick, N., eds., Strike-slip deformation, basin formation and sedimentation: Society of Economic Paleontologists and Mineralogist Special Publication 17, p. 227–264.

Şengör, A.M.C., Tüysüz, O., İmren, C., Sakınç, M., Eyidoğan, H., Görür, N., Le Pichon, X., and Rangin, C., 2005, The North Anatolian fault: A new look: Annual Review of Earth and Planetary Sciences, v. 33, p. 37–112, doi: 10.1146/annurev.earth.32.101802.120415.

Seyitoğlu, G., and Scott, B., 1992, Late Cenozoic volcanic evolution of the northeastern Aegean region: Journal of Volcanology and Geothermal Research, v. 54, p. 157–176, doi: 10.1016/0377-0273(92)90121-S.

Sherlock, S., Kelley, S.P., Inger, S., Harris, N., and Okay, A.I., 1999, ^{40}Ar-^{39}Ar and Rb-Sr geochronology of high-pressure metamorphism and exhumation history of the Tavsanli zone, NW Turkey: Contributions to Mineralogy and Petrology, v. 137, p. 46–58.

Spear, F.S., Kohn, M.J., and Cheney, J.T., 1999, *P-T* paths from anatectic pelites: Contributions to Mineralogy and Petrology, v. 134, p. 17–32, doi: 10.1007/s004100050466.

Straub, C., 1996, Recent crustal deformation and strain accumulation in the Marmara Sea region, N.W. Anatolia, inferred from GPS measurements [Ph.D. thesis]: Zürich, Swiss Federal Institute of Technology, 123 p.

Tapponnier, P., Lacassin, R., Leloup, P.H., Scharer, U., Zhong, D.L., Wu, H.W., Liu, X.H., Ji, S.C., Zhang, L.S., and Zhong, J.Y., 1990, The Ailao Shan Red River metamorphic belt—Tertiary left-lateral shear between Indochina and South China: Nature, v. 343, p. 431–437, doi: 10.1038/343431a0.

Thomson, N., and Ring, U., 2006, Thermochronologic evaluation of postcollision extension in the Anatolide orogen, western Turkey: Tectonics, v. 25, TC3005, doi: 10.1029/2005TC001833

Tokay, F., and Altunel, E., 2005, Neotectonic activity of Eskişehir fault zone in vicinity of İnönü–Dodurga area: Bulletin of the Mineral Research and Exploration Institute of Turkey, v. 130, p. 1–15.

Turhan, N., 2002, Geological map of Turkey, Ankara Sheet: Ankara, Maden Tetkik ve Arama Genel Müdürlüğü, scale 1:500,000, 1 sheet.

Uysal, I.T., Mutlu, H., Altunel, E., Karabacak, V., and Golding, S.D., 2006, Clay mineralogical and isotopic (K-Ar, $\delta^{18}O$, δD) constraints on the evolution of the North Anatolian fault zone, Turkey: Earth and Planetary Science Letters, v. 243, p. 181–194, doi: 10.1016/j.epsl.2005.12.025.

van der Kaaden, G., 1958, On the genesis and mineralisation of the tungsten deposit Uludağ: Bulletin of the Mineral Research and Exploration Institute of Turkey, v. 50, p. 33–43.

Walcott, R.I., 1998, Modes of oblique compression: Late Cenozoic tectonics of the South Island of New Zealand: Reviews of Geophysics, v. 36, p. 1–26, doi: 10.1029/97RG03084.

Yaltırak, C., 2002, Tectonic evolution of the Marmara Sea and its surroundings: Marine Geology, v. 190, p. 493–529, doi: 10.1016/S0025-3227(02)00360-2.

Yıldırım, C., Emre, Ö., and Doğan, A., 2005, The uplift of the Uludağ Massif and the Bursa and Uludağ faults, *in* Workshop on the Seismicity of the Eskişehir fault zone and Related systems, Abstracts: Eskişehir, Eskişehir Osmangazi University, p. 8 (in Turkish).

Yılmaz, Y., 1993, New evidence and model on the evolution of the southeast Anatolian orogen: Geological Society of America Bulletin, v. 105, p. 251–271, doi: 10.1130/0016-7606(1993)105<0251:NEAMOT>2.3.CO;2.

Yılmaz, Y., Genç, Ş.C., Karacık, Z., and Altunkaynak, Ş., 2001, Two contrasting magmatic associations of NW Anatolia and their tectonic significance: Journal of Geodynamics, v. 31, p. 243–271, doi: 10.1016/S0264-3707(01)00002-3.

Zattin, M., Landuzzi, A., Picotti, V., and Zuffa, G.G., 2000, Discriminating between tectonic and sedimentary burial in a foredeep succession, Northern Apennines: Journal of the Geological Society [London], v. 157, p. 629–633.

Zattin, M., Okay, A.I., and Cavazza, W., 2005, Fission-track evidence for late Oligocene and mid-Miocene activity along the North Anatolian fault in southwestern Thrace: Terra Nova, v. 17, p. 95–101, doi: 10.1111/j.1365-3121.2004.00583.x.

Manuscript received 16 March 2007
Revised manuscript received 18 November 2007
Manuscript accepted 8 December 2007

Printed in the USA